Metabolic diversity in commensal protists regulates intestinal immunity and trans-kingdom competition

Elias R. Gerrick[1], Soumaya Zlitni[2,3,9], Patrick T. West[2,3,9], Claire M. Mechler[1], Jessica A. Li[1], Steven K. Higginbottom[4], Christopher J. Severyn[2,5], Frauke Kracke[6], Alfred M. Spormann[6,7], Justin L. Sonnenburg[4,8], Ami S. Bhatt[2,3], Michael R. Howitt[1,4,10,*]

[1]Department of Pathology, Stanford University School of Medicine, Stanford, CA 94305, USA

[2]Department of Genetics, Stanford University, Stanford, CA 94305, USA

[3]Department of Medicine, Stanford University School of Medicine, Stanford, CA 94305, USA

[4]Department of Microbiology and Immunology, Stanford University School of Medicine, Stanford, CA 94305, USA

[5]Department of Pediatrics, (Division of Hematology/Oncology/Stem Cell Transplant and Regenerative Medicine), Stanford University, Palo Alto, CA , 94305, USA

[6]Department of Civil and Environmental Engineering, Stanford University, Stanford, CA 94305, USA

[7]Department of Chemical Engineering, Stanford University, Stanford, CA 94305, USA

[8]Chan Zuckerberg Biohub, San Francisco, CA 94158, USA

[9]These authors contributed equally

[10]Lead contact

*Correspondence: mhowitt@stanford.edu

Keywords

Commensal protist; Tritrichomonas; parabasalid; microbiome; trans-kingdom; mucus; fiber; microbiota-accessible carbohydrate; metabolites; tuft cell

Summary

Protists in the gut microbiota influence intestinal immunity and epithelial composition, yet the mechanisms used by these protists to shape the gut environment remain poorly understood. Here, we identify a new protist species, *Tritrichomonas casperi,* and show that metabolic differences between closely related commensal protists modulate their effects on host immunity and determine their ecological niche within the murine microbiota. Genomic and metabolomic analysis of commensal tritrichomonads reveal species-level differences in excretion of the tuft cell activating metabolite succinate, leading to differential induction of Th1, Th2, and Th17 cells in the small intestine. Using defined diets and *in vitro* growth assays, we show that different tritrichomonad species preferentially rely on dietary polysaccharides or mucus glycans, which leads to trans-kingdom competition with specific bacteria in the microbiota. Our findings elucidate differences in commensal tritrichomonad metabolism and suggest how dietary interventions could regulate the impact of these protists on gut health.

52 **Introduction**

53 The gut microbiota is a complex and diverse microbial ecosystem that broadly impacts
54 the development and function of the intestinal immune system (Chu and Mazmanian, 2013;
55 Hooper et al., 2012; Kamada et al., 2013; Littman and Pamer, 2011; Rooks and Garrett, 2016).
56 This relationship has been studied predominately at the microbial community level, where
57 conserved microbial ligands and metabolites have pleiotropic effects on the host (Atarashi et al.,
58 2013; Belkaid and Hand, 2014; Levy et al., 2015; Smith et al., 2013; Zheng et al., 2019).
59 However, some microbial species dominantly influence the immune system independent of
60 other microbiota members (Bae et al., 2022; Ivanov et al., 2009; Mazmanian et al., 2008). For
61 example, segmented filamentous bacteria (SFB) are sufficient to induce T helper 17 (Th17) cells
62 in the murine small intestine, and *Bacteroides fragilis* stimulates regulatory T cells in the colon
63 (Ivanov et al., 2009; Mazmanian et al., 2008). While bacteria are the most well-characterized
64 immunologically dominant members of the gut microbiota, this community also contains viruses,
65 fungi, archaea, and protists that interact with the host and alter immunological function.

66 Protists are often overlooked as members of the microbiota, in part due to the historical
67 view of these microbes as universally pathogenic. However, protists are present in healthy
68 mammalian guts, including those of mice and humans (Billy et al., 2021; Chudnovskiy et al.,
69 2016; Clemente et al., 2012; Lukeš et al., 2015; Parfrey et al., 2014). Commensal parabasalid
70 protists from the genus *Tritrichomonas* are widespread in laboratory mice and dramatically alter
71 the gut mucosa (Chudnovskiy et al., 2016; Howitt et al., 2016; Nadjsombati et al., 2018;
72 Schneider et al., 2018). In the small intestine, *Tritrichomonas* species drive type 2 immunity
73 through production of the metabolite succinate, which lengthens the gut and promotes tuft and
74 goblet cell hyperplasia in the epithelium (Nadjsombati et al., 2018; Schneider et al., 2018). In the
75 colon, *Tritrichomonas musculis* (*Tmu*) activates the inflammasome to promote Th1 and Th17
76 immunity (Chudnovskiy et al., 2016; Escalante et al., 2016). These tritrichomonads do not
77 induce apparent pathology, but they significantly alter host susceptibility to enteric infections and

78 increase the severity of several inflammatory diseases through their effects on intestinal
79 epithelial and immune functions (Chudnovskiy et al., 2016; Escalante et al., 2016; Nadjsombati
80 et al., 2018; Schneider et al., 2018). Despite the growing appreciation of commensal
81 tritrichomonads as immunologically dominant species that impact mucosal tissues, very little is
82 understood about their diversity, metabolism, or microbial ecology.

83 Answering fundamental questions regarding commensal tritrichomonad protists is
84 impeded by a lack of genomic information and their resistance to *in vitro* culture. Consequently,
85 the biology of commensal *Tritrichomonas* species is largely inferred from studies on the
86 urogenital pathogenic parabasalids *Trichomonas vaginalis* and *Tritrichomonas foetus.* However,
87 these pathogens infect different hosts and anatomical niches that may not reflect the specific
88 adaptations of commensal tritrichomonads in the gut. In addition, the ecological role of
89 commensal tritrichomonads within the murine gut microbiota is unexplored. Parabasalid protists
90 are generally fermentative (Brune, 2014; Muller et al., 2012; Petrin et al., 1998; Schneider et al.,
91 2018), but the specific carbohydrate sources used by commensal tritrichomonads and how
92 harvesting of these carbohydrates affects their interactions with the bacterial members of the
93 microbiota and the host is unknown.

94 In this work, we use genomic, transcriptomic, and metabolomic approaches to show that
95 differences in fermentative output between two commensal *Tritrichomonas* species drive
96 divergent immune responses in the murine intestine. Further, we demonstrate that these
97 different species' preferences for fermenting plant polysaccharides or mucus glycans affect
98 trans-kingdom interactions with bacteria. Finally, through highly controlled studies on
99 carbohydrate utilization, we reveal that dietary manipulation can act as a lever to control protist-
100 induced immunomodulation. Our work provides mechanistic insights into how commensal
101 tritrichomonads, through their metabolic differences, act as architects of the intestinal
102 ecosystem and establishes a foundation for further mechanistic studies of how these protists
103 influence both host immunity and microbiome ecology.

104 **RESULTS**

105 **Discovery of a new commensal *Tritrichomonas* species in mice**

106 To discover uncharacterized parabasalid protists within laboratory mice, we collected
107 stool from across the Stanford University animal facilities and screened DNA extracted from
108 these samples using pan-parabasalid PCR primers. These primers bind to highly conserved
109 sequences of parabasalid rRNA loci and generate internally transcribed spacer (ITS) amplicons
110 sufficient to distinguish parabasalid species using Sanger Sequencing. As expected, we
111 identified *Tmu* in a subset of our mice, but stool from another subset of mice produced mixed
112 signal in specific regions of the ITS sequence. This pattern is consistent with the amplification of
113 multiple closely related sequences in the PCR reaction, leading us to suspect that these mice
114 were colonized by more than one species of protist. Examination of the cecal contents of these
115 mice by light microscopy revealed protists with two distinct sizes: a large variant consistent in
116 size with *Tmu*, and another variant approximately half the length.

117 To determine if these two sizes constitute different morphologies of *Tmu* or two separate
118 species, we purified both sizes of protist by fluorescence-activated cell sorting (FACS) and
119 colonized protist-negative specific pathogen free (SPF) mice with either the large or small
120 variant (Figure 1A). Mice maintained stable colonization with homogenously small or large
121 protists, as verified by scanning electron microscopy (SEM), suggesting these were indeed
122 separate species (Figure 1B and 1C). Ultrastructural examination of both protists revealed an
123 undulating membrane and recurrent flagellum typical of the *Parabasalia* phylum (Figure 1B)
124 (Cepicka et al., 2010). SEM also suggested that the new protist, like *Tmu,* is a member of the
125 genus *Tritrichomonas*, based on the presence of three anterior flagella. To confirm this
126 phylogenetic relationship, we compared ITS sequences from both protists, which revealed the
127 smaller species as an uncharacterized murine isolate with the accession number MF375342
128 that shares 83.39% identity with *Tmu* (Figure 1D and S1A). Thus, the smaller protist is a new
129 species, which we hereafter refer to as *Tritrichomonas casperi* (*Tc*).

130 All previously characterized commensal tritrichomonads, including *Tmu*, induce tuft cell
131 hyperplasia and type 2 immunity in the distal small intestine (SI) through excretion of the
132 metabolite succinate (Escalante et al., 2016; Howitt et al., 2016; Nadjsombati et al., 2018;
133 Schneider et al., 2018). However, tuft cell hyperplasia was absent in mice colonized with *Tc* as
134 assessed by both flow cytometry and microscopy (Figure 1E and 1F). Moreover, *Tc* colonization
135 reduced the proportion of small intestinal GATA3^{+} CD4^{+} T helper 2 (Th2) cells associated with
136 type 2 immunity, which contrasts with the marked expansion of Th2 cells in the lamina propria of
137 *Tmu* colonized mice (Figure 1G). To determine whether *Tc* fails to drive type 2 immunity
138 because of colonization deficiencies, we compared *Tc* and *Tmu* abundance by quantitative
139 PCR. *Tc* was at least as abundant as *Tmu* in the distal SI, cecum, and colon (Figure S1B).
140 These results suggest that *Tc* is unique among known murine commensal tritrichomonads for its
141 lack of type 2 immune induction in the distal SI.
142
143 **T cell responses to *Tmu* and *Tc* differ in the small intestine but are similar in the colon**
144 Previous work demonstrated that *Tmu* increases CD4^{+} T helper 1 (Th1) and T helper 17
145 (Th17) cells in the cecum and colon (Chudnovskiy et al., 2016; Escalante et al., 2016). We
146 therefore examined whether *Tc* stimulates these same immune responses in the distal SI. IFNγ
147 producing Th1 cells and IL-17 producing Th17 cells significantly increased in the distal SI of *Tc*
148 colonized mice compared to protist-free controls (Figure 2A and 2B). Because *Tmu* instead
149 stimulates Th2 cells in the distal SI, we wondered whether co-colonization would alter the
150 mucosal response to these protists. To address this question, we co-colonized mice with *Tmu*
151 and *Tc* or singly with each protist and compared tuft cell frequencies as a marker of type 2
152 immunity in the distal SI. Tuft cell hyperplasia was identical in co-colonized and *Tmu* singly
153 colonized mice, and *Tc* and *Tmu* abundance was unaffected by co-colonization (Figure S2A and
154 S2B). This finding suggests that *Tmu* has a dominant effect on the mucosal immune response
155 when both species are present simultaneously in the distal SI.

156 Although *Tmu* induces Th1 and Th17 cells in the colon and type 2 immunity in the distal
157 SI, no study has examined the immune response in both intestinal tissues using the same
158 protist isolate. This leaves some ambiguity concerning the contribution of strain or species
159 differences to these heterogeneous immune responses. We therefore characterized $CD4^+$ T cell
160 populations induced by *Tmu* and *Tc* in the colon. Both *Tmu* and *Tc* individually stimulated a
161 significant increase in the number and proportion of Th1 and Th17 cells (Figure 2C and 2D).
162 These results suggest that *Tmu* induces regionally specific $CD4^+$ T cell responses, while *Tc*
163 impacts the T cell compartment homogenously across the gut. Microbial adhesion has been
164 proposed as a nonspecific Th17-inducing signal in the distal SI (Atarashi et al., 2015), and
165 previous work has identified examples of *Tmu* adhering to colonic epithelial cells (Chudnovskiy
166 et al., 2016). To address the prevalence of epithelial adhesion by *Tmu* and *Tc* in the distal SI
167 and colon, we developed a polyclonal antibody against *Tmu*. This antibody recognizes *Tmu*
168 and, to a lesser extent, *Tc*, and is capable of staining both trophozoites and pseudocysts of *Tmu*
169 (Figure S2C and S2D). Although both protists could be found near the epithelial barrier at high
170 densities, the mucus layer physically separated the protists from the host (Figure 2E and 2F).
171 To determine if small sub-populations of protists adhere to the epithelium, we gently flushed the
172 colons of *Tmu*-colonized mice to remove unadhered protists and then searched for adherent
173 *Tmu* by microscopy. While we could identify adherent protists, these were extremely rare events
174 (1-3 per colonic tissue section) and are unlikely to drive immune responses across the entire
175 tissue (Figure S2E and S2F).
176
177 **Metabolic differences in tritrichomonads underly divergent immune responses**
178 Succinate excreted by *Tmu* stimulates the succinate receptor (GPR91) on tuft cells and
179 drives type 2 immunity in the distal SI (Figure S3A) (Nadjsombati et al., 2018; Schneider et al.,
180 2018). Because tuft cell hyperplasia and type 2 immunity are absent in *Tc* colonized mice, we
181 hypothesized that *Tc* does not produce succinate as a metabolic waste product. To directly

182 measure *in vivo* succinate concentrations during *Tmu* and *Tc* colonization, we used liquid
183 chromatography-mass spectrometry (LC-MS) to quantify this metabolite in the extracellular
184 fraction of mouse cecal contents. *Tmu* colonization led to significantly higher concentrations of
185 cecal succinate than controls, while *Tc* colonized mice showed no change in succinate levels
186 (Figure 3A).

187 Two metabolic paradigms are currently known for parabasalid protists, based on
188 previous studies of *Trichomonas vaginalis* and *Tritrichomonas foetus* (Muller et al., 2012;
189 Westrop et al., 2017). These species are also anaerobic and generate ATP through glycolysis,
190 which converts NAD^+ to NADH. Without oxidative respiration, NADH accumulates and must be
191 converted back to NAD^+ through a fermentative pathway to maintain redox homeostasis. In *T.*
192 *vaginalis* this is accomplished by converting pyruvate to lactate through the action of lactate
193 dehydrogenase. In *T. foetus,* and presumably *Tmu*, NAD^+ regeneration occurs via conversion of
194 malate to succinate by the sequential activity of fumarase and fumarate reductase. Lactate or
195 succinate are then excreted as waste products from the protists. However, as with succinate, *Tc*
196 colonization did not result in an increase in extracellular lactate in mouse cecal contents (Figure
197 S3B).

198 To identify the metabolic pathways present in each protist, we sequenced the genomes
199 of both *Tmu* and *Tc*. Massive numbers of transposable elements and repeat regions in
200 parabasalid genomes convolute genomic assemblies using traditional Next-Generation
201 Sequencing approaches (Barratt et al., 2016; Carlton et al., 2007; Palmieri et al., 2021).
202 Therefore, we used Nanopore long-read sequencing and short-read error correction to
203 assemble these parabasalid genomes (Figure 3B, 3C, and S3C). We next annotated and mined
204 the newly assembled *Tmu* and *Tc* genomes to determine the fermentative pathways present in
205 each species. As predicted, *Tmu* encodes the succinate production pathway, but not the lactate
206 pathway (Figure 3D, blue box). Despite the lack of succinate or lactate excretion by *Tc*, it
207 encodes both the succinate and lactate production genes (Figure 3D, red boxes). To assess the

208 relative contribution of each of these pathways to *Tc* metabolism, we performed RNA
209 sequencing (RNA-seq) on *Tmu* and *Tc* isolated from the distal SI and ceca of mice. *Tmu* and *Tc*
210 both expressed genes in the succinate pathway at high levels, whereas lactate dehydrogenase
211 was less highly expressed in *Tc* (Figure 3E and 3F). Additionally, *Tmu* and *Tc* transcriptomes
212 confirmed that fermentative pathways leading to succinate or lactate production do not vary
213 drastically between the distal SI and cecum (Figure 3E and 3F). Together, these genomic and
214 transcriptomic data suggest that *Tmu* and *Tc* both use the succinate fermentation pathway,
215 contrary to our hypothesis based on LC-MS measurements from cecal contents and the lack of
216 type 2 immune induction by *Tc*.

217 To directly determine the usage of each fermentative pathway in *Tmu* and *Tc*, we next
218 measured the intracellular concentrations of both metabolites in purified protists. Consistent with
219 the genomic and transcriptomic analyses, cell extracts from purified *Tmu* and *Tc* had high levels
220 of succinate and low levels of lactate (Figure 3G and 3H). These intracellular succinate
221 concentrations suggest that both protists use the succinate pathway to maintain metabolic redox
222 homeostasis, yet cecal LC-MS measurements and the absence of tuft cell hyperplasia suggest
223 *Tc* does not release this metabolite into the intestinal space. Some bacteria can metabolize
224 succinate into short chain fatty acids such as propionate and butyrate (Ferreyra et al., 2014;
225 Fischbach and Sonnenburg, 2011). Therefore, we reasoned that *Tc* might also metabolize
226 succinate in a similar manner. However, the short chain fatty acids butyrate, propionate, and
227 acetate were unchanged in the cecal contents of *Tc* colonized mice compared with uncolonized
228 controls (Fig. S3D). Altogether, these data indicate that both protists use succinate production to
229 maintain redox homeostasis, but *Tmu* excretes succinate as a waste product whereas *Tc* may
230 shunt succinate into an alternative metabolic pathway.

231 We observed that *T. foetus*, *Tmu*, and *Tc* all use the succinate pathway for redox
232 balance and belong to the class *Tritrichomonadea*. *T. vaginalis* alternatively uses the lactate
233 pathway for redox balance and belongs to the class *Trichomonadea*. This led us to hypothesize

234 that an evolutionary split had occurred within the *Parabasalia* phylum, with lactate versus
235 succinate production representing a branch point. To investigate this hypothesis, we analyzed
236 the fermentative metabolism of two additional intestinal parabasalids: *Pentatrichomonas*
237 *hominis* (a human-associated *Trichomonadea*) and *Monocercomonas colubrorum* (a reptile-
238 associated *Tritrichomonadea*) (Figure 3I). As predicted, *P. hominis* cultures contained high
239 concentrations of lactate whereas *M. colubrorum* cultures contained high concentrations of
240 succinate (Figure 3I and S3E). These data suggest that the phylogenetic classification of new
241 and uncharacterized parabasalid species can help predict their production of the
242 immunomodulatory metabolites lactate and succinate.
243

244 **_Tmu_ and _Tc_ occupy different nutritional niches within the microbiota**

245 Although the microbiota's metabolic output dramatically affects the gut ecosystem, the
246 metabolic input of each species also shapes its interactions with other microbes and the host
247 (Coyte and Rakoff-Nahoum, 2019; Park et al., 2022; Tuncil et al., 2017). Plant polysaccharides
248 that are undigested by host enzymes in the proximal intestine, such as dietary fibers, are the
249 most commonly utilized carbon source by the microbiota, and collectively these glycans are
250 termed dietary Microbiota Accessible Carbohydrates (MACs) (Porter, Nathan T and Martens,
251 Eric C, 2017; Sonnenburg and Sonnenburg, 2014; Wardman et al., 2022). However, non-dietary
252 MACs are also prevalent in the intestine. For example, mucus secreted by goblet cells in the
253 intestinal epithelium provides a complex and glycan-rich nutrient source for microbes capable of
254 breaking down its diverse glycosidic linkages (Desai et al., 2016; Tailford et al., 2015; Wardman
255 et al., 2022). To determine whether *Tmu* and *Tc* ferment dietary MACs, we altered the fiber
256 content of mouse diets using defined chow similar to a previous study (Schneider et al., 2018).
257 Fibers in these diets were restricted to inulin, a fermentable fiber that acts as a dietary MAC,
258 and cellulose, a non-fermentable fiber that acts as a bulking agent and passes largely
259 undigested through the intestine. *Tmu* abundance was high in mice fed defined chow (inulin and

260 cellulose) and inulin-only diets (Figure 4A and S4A). However, when fiber was removed entirely
261 or cellulose was the sole fiber, *Tmu* colonization was dramatically reduced (Figure 4A and S4A).
262 Thus, *Tmu* colonization depends on dietary MACs. In contrast, *Tc* colonization was completely
263 independent of these dietary glycans, as protist abundance was unaffected on any of the four
264 diets (Figure 4B, S4B). These results suggest that *Tc* may rely on host-derived carbohydrates
265 as a nutritional source.

266 The gut microbial ecosystem is a complex and species rich community, with most
267 nutritional niches occupied by one or more community members competing for limited resources
268 (Coyte et al., 2015; Coyte and Rakoff-Nahoum, 2019; Patnode et al., 2019). This scarcity of
269 open niches occludes new microbes from colonizing the gut and establishing themselves in the
270 community, a phenomenon termed “colonization resistance”. However, commensal
271 tritrichomonads such as *Tmu* and *Tc* are unusual compared to many commensal bacteria in that
272 they appear unaffected by colonization resistance. As few as one thousand *Tmu* or *Tc* protists
273 can stably colonize SPF mice without antibiotic pre-treatment or other niche-clearing
274 manipulation. We reasoned that *Tmu* and *Tc* could overcome colonization resistance due to one
275 of two possibilities, (1) *Tmu* and *Tc* occupy unique niches that no other member of the
276 microbiota inhabits, or (2) *Tmu* and *Tc* are adept at outcompeting other microbes that occupy
277 their preferred niche. Due to the dearth of unoccupied niches in the gut ecosystem, we favored
278 the second hypothesis that these tritrichomonads displace other members of the microbiota to
279 establish colonization. Therefore, identifying microbes eliminated by tritrichomonad colonization
280 could offer insights into the nutritional niches occupied by *Tmu* and *Tc*.

281 To investigate trans-kingdom competition between tritrichomonads and bacteria, we
282 analyzed the effects of *Tmu* and *Tc* on the bacterial compartment of the microbiome using 16S
283 rRNA sequencing (Figure 4C and S4C). Colonization by both *Tmu* and *Tc* was associated with
284 small but significant decreases in total bacterial abundance, supporting the hypothesis that
285 these protists displace bacterial competitors (Figure S4D). However, *Tmu* colonization did not

286 change bacterial alpha-diversity, and *Tc* colonization increased alpha-diversity, suggesting that
287 these protists engage in complex trans-kingdom interactions that are not universally
288 antagonistic (Figure S4E). We performed LEfSe analysis to identify differentially abundant
289 bacterial clades influenced by tritrichomonad colonization (Segata et al., 2011). Unlike the
290 microbiota of *Tmu* colonized mice, *Tc* colonization was associated with a dramatic reduction in
291 the relative abundance of just two bacteria: an undefined member of the *Bacteroidales* order,
292 and *Akkermansia muciniphila* (Figure 4D and Figure S4F). Many *Bacteroidetes* ferment mucus
293 glycans, and *A. muciniphila* is a well-documented mucus specialist that uses mucus glycans as
294 its primary source of carbohydrates (Derrien et al., 2004; Desai et al., 2016; Martens et al.,
295 2008; Sonnenburg, 2005). To confirm that *Tc* colonization displaces *A. muciniphila*, we verified
296 the dramatic decrease of this species by qPCR (Figure 4E). Taken together, these dietary and
297 trans-kingdom competition experiments suggest that *Tmu* ferments dietary MACs, while *Tc*
298 instead ferments host-derived carbohydrates from mucin glycoproteins.
299 Mucus proteins are decorated with diverse glycan structures that require a large
300 repertoire of carbohydrate active enzymes (CAZymes) to digest. To investigate the glycan
301 utilization potential of *Tmu* and *Tc*, we used dbCAN2 to identify CAZymes in the protist
302 transcriptomes (Zhang et al., 2018). Consistent with *Tc* fermenting mucus glycans, we identified
303 highly expressed CAZymes with putative mucolytic activity in *Tc* (Figure 4F) (Lombard et al.,
304 2014; Smits et al., 2017; Wardman et al., 2022). *Tc* expresses CAZymes with predicted activity
305 against all of the sugar subunits found on mucus glycans, and these CAZymes are members of
306 Glycoside Hydrolase (GH) families associated with mucus degradation (Figure 4F) (Desai et al.,
307 2016; Smits et al., 2017). In particular, *Tc* expresses high levels of galactosidases, which can
308 cleave the abundant galactose residues from mucus glycans. Unlike glucose, no direct catabolic
309 pathway exists for galactose utilization, and thus this monosaccharide must be converted to
310 glucose to be oxidized for energy production. Consistent with a galactose-dependent
311 metabolism, *Tc* also expresses high levels of the enzyme UDP-galactose 4-epimerase, which is

312 essential for galactose conversion to glucose (Holden et al., 2003). However, these putatively
313 mucolytic CAZymes identified in *Tc* are also found in *Tmu*, albeit at lower relative abundance,
314 suggesting that *Tmu* may also be capable of fermenting mucus glycans (Figure 4F).
315
316 **Dietary MAC deprivation causes *Tmu* to switch to mucolytic metabolism**
317 Although *Tmu* colonization was markedly reduced when mice were fed the cellulose diet,
318 a small number of protists survived in a subset of these mice (Figure 4A and S4A). This
319 observation, combined with the expression of putative mucolytic CAZymes, suggested that *Tmu*
320 can utilize mucus glycans to survive dietary MAC deprivation. To investigate this possibility, we
321 examined the localization of *Tmu* in the intestines of mice fed cellulose as the sole fiber. As
322 expected, dramatically fewer *Tmu* were visible in the colons of cellulose-fed mice than mice fed
323 normal mouse chow (complex chow), which contains a wide variety of dietary MACs (Figure
324 5A). The few remaining *Tmu* cells in cellulose-fed mice strongly co-localized with the mucus
325 layer (Figure 5A, right), supporting our hypothesis that *Tmu* survives dietary MAC deprivation by
326 fermenting mucus glycans.
327 We next sought to study this metabolic shift in a reductionist model to understand the
328 effects of specific substrates on protist growth and survival without the inherent complexity of
329 the intestinal environment. Although some parabasalid species can be propagated *in vitro*,
330 murine gut commensals such as *Tmu* and *Tc* do not grow with existing culture conditions.
331 Although previous studies by our group and others have cultured these protists short-term to
332 eliminate bacteria and fungi with antibiotics (Chudnovskiy et al., 2016; Howitt et al., 2016;
333 Nadjsombati et al., 2018; Schneider et al., 2018), growth does not occur; instead, the protists
334 slowly die over the course of several days. This method is sufficient to colonize mice with pure
335 protists, but it does not allow for the investigation of protist biology. We therefore attempted to
336 develop *in vitro* culture conditions for *Tmu* and *Tc,* which would allow for mechanistic
337 interrogation of their metabolisms. We successfully modified existing parabasalid growth

338 formulations to create new culture conditions, which we named PBF medium, that allow for
339 long-term propagation of *Tmu* (Figure S5A). Despite the success of PBF medium for *Tmu*
340 culture, this new medium did not support the growth of *Tc*. Nevertheless, adding mucus to PBF
341 medium improved *Tc* survival 5-fold, supporting the hypothesis that this species ferments
342 mucus glycans (Figure S5B).

343 Using the newly developed PBF medium, we cultured *Tmu* axenically with either the
344 simple sugar maltose or with mucus as the primary carbon source, and found that both glycans
345 supported robust growth of the protist (Figure 5B). We next used this reductionist system to
346 confirm whether the CAZymes identified above (Figure 4F) are involved in mucus glycan
347 harvesting by *Tmu* and *Tc* by performing transcriptomics on *Tmu* grown with either maltose or
348 mucus (Figure 5C). Differential expression analysis revealed *Tmu* grown with mucus
349 significantly increased expression of 16 CAZymes in GH families associated with mucolytic
350 activity relative to protists grown in maltose cultures. This upregulated set of CAZymes included
351 the putative mucolytic genes identified above, supporting the hypothesis that both protists use
352 these CAZymes to metabolize mucus glycans. In addition, the gene encoding the galactose-
353 utilization enzyme UDP-galactose-4-epimerase was upregulated in mucus-grown *Tmu,*
354 suggesting a metabolic shift towards fermentation of mucosal sugars.

355 The discrepancy between *Tmu* survival on mucus *in vivo* (in which the protists barely
356 survive) and *in vitro* (where the protists thrive) led us to consider what factors might account for
357 this difference. One major distinction between these two systems is the absence of bacteria in
358 the *in vitro* cultures. To determine if mucolytic bacteria outcompete *Tmu* during dietary MAC
359 deprivation *in vivo*, we treated *Tmu*-colonized mice with antibiotics before switching to the
360 cellulose diet. Strikingly, antibiotic treatment with a cocktail of vancomycin, neomycin, and
361 ampicillin restored *Tmu* colonization in the absence of dietary MACs (Figure 5D and S5C). To
362 narrow down the potential bacterial competitors, we tested the ability of each individual antibiotic
363 to restore colonization in mice fed cellulose diets. Neomycin and vancomycin were dispensable

364 for *Tmu* survival, whereas ampicillin treatment alone completely restored colonization (Figure
365 5E and S5D).
366 We next sought to identify specific bacteria that outcompete *Tmu* during dietary MAC
367 starvation by profiling the changes to the bacterial microbiota during treatment with each of the
368 individual antibiotics. Mice treated with ampicillin had undetectable levels of *Bacteroidetes* and
369 *Akkermansia muciniphila*, known mucolytic members of the microbiota, which were also the
370 groups outcompeted by *Tc* (Figure 5F, 5G, and S5E). In contrast, the mice treated with no
371 antibiotics, vancomycin, or neomycin all had high levels of *Bacteroidetes*, *Akkermansia*, or both
372 bacteria (Figure 5F, 5G, and S5E). These results suggest that *Tmu* switches to a mucolytic
373 metabolism during dietary MAC starvation, but is largely outcompeted by the mucolytic bacteria
374 *Bacteroides spp*. and *A. muciniphila*.
375
376 **Diet-protist interactions shape the host immune response**
377 Next, we characterized dietary MAC fermentation by *Tmu* using axenic *in vitro* culture.
378 Dietary MACs appear to be the preferred fermentative substrate of this species, and inulin
379 specifically was sufficient for *Tmu* to colonize mice (Figure 4A). However, *Tmu* failed to grow in
380 PBF medium when inulin was provided as the carbon source (Figure 6A). To understand this
381 apparent discrepancy, we compared the spatial localization of *Tmu* in mice fed either normal
382 mouse chow, which has a varied, undefined mixture of dietary MACs (complex chow), and the
383 defined mouse chow with inulin as the sole dietary MAC. As expected, we found *Tmu* both at
384 the mucosal interface and dispersed throughout the lumen in mice fed complex chow (Figure
385 6B, left). However, when mice were fed defined chow, the protists were tightly associated with
386 the mucus layer and largely absent from the intestinal lumen (Figure 6B, middle). This
387 enrichment of *Tmu* near the mucus layer was similar to *Tmu* in cellulose-fed mice (Figure 6B,
388 right), although the overall abundance of protists was markedly higher with the inulin-containing
389 defined chow. This suggests that although the addition of inulin is sufficient for *Tmu* to colonize

390 mice at high abundance, *Tmu* does not directly utilize inulin and instead ferments mucus
391 glycans when inulin is the sole dietary MAC. Notably, many *Bacteroidetes* species can ferment
392 both inulin and mucus, suggesting that these bacteria may utilize inulin when the fiber is
393 present, thereby reducing competition with *Tmu* for mucus glycans (Desai et al., 2016;
394 Sonnenburg et al., 2010). *Bacteroidetes* abundance did not change in *Tmu*-colonized mice fed
395 cellulose chow compared to defined chow, whereas *Tmu* levels decreased in cellulose chow
396 (Figure 6C, left and 4A). This observation is consistent with *Bacteroidetes* outcompeting *Tmu* for
397 mucus glycans when all dietary MACs, including inulin, are removed. However, this same
398 dietary switch in *Tc*-colonized mice results in a significant decrease in *Bacteroidetes*
399 abundance, consistent with the ability of *Tc* to outcompete these bacteria for the mucus niche
400 (Figure 6C).
401 To determine whether *Tmu* can ferment dietary MACs, we tested a wider array of
402 fermentable fibers as the carbon source in *Tmu* cultures. While *Tmu* failed to grow in maltose-
403 free PBF medium supplemented with the fibers arabinan, arabinogalactan, and
404 fructooligosacharides (FOS), the protist readily grew on arabinoxylan, galactomannan, and
405 pectin (Figure 6D and S6A). Thus, similar to the bacterial fiber-consuming members of the
406 microbiota, *Tmu* ferments dietary MACs but can only utilize specific glycan structures. To
407 identify the CAZymes responsible for fiber utilization by *Tmu*, we performed transcriptomics on
408 *Tmu* cultured with either the simple sugar maltose or the fermentable fiber arabinoxylan (Figure
409 6E). We identified 3 CAZymes in GH families associated with fiber utilization that exhibited
410 increased expression during growth on arabinoxylan, suggesting that *Tmu* uses these CAZymes
411 to break down fiber polymers (Figure 6E) (Desai et al., 2016; Smits et al., 2017).
412 Finally, we wondered whether diet and *Tmu* metabolic input would affect immune
413 induction by the protist. When *Tmu*-colonized mice were fed the defined chow, and thus *Tmu*
414 fermented mucus glycans, type 2 immune induction was suppressed (Figure 6F). This
415 suppression did not appear to be due to decreased succinate output by *Tmu* on a per-cell basis

416 during mucus feeding, as *Tmu* grown on mucus *in vitro* showed no decrease in succinate
417 excretion (Figure S6B). However, *Tmu* abundance in the distal SI of mice fed defined chow was
418 substantially lower, suggesting that when fermenting mucus, this protist cannot colonize the SI
419 at sufficiently high levels to induce type 2 immunity (Figure 6G).
420

421 **Discussion**

422 Parabasalid protists, including tritrichomonads, are relatively common in the
423 microbiomes of both feral and laboratory mice and can be found in the microbiomes of healthy
424 humans (Lukeš et al., 2015; Parfrey et al., 2014, 2011; Stark et al., 2016). In animal studies,
425 commensal tritrichomonads powerfully influence mucosal immunity and intestinal epithelial
426 differentiation, resulting in significant protection from co-infections with enteric pathogens, but
427 with exacerbation of certain chronic inflammatory diseases (Chudnovskiy et al., 2016; Escalante
428 et al., 2016; Schneider et al., 2018). Despite their emergence as immunodominant members of
429 the microbiota, little is known about the biology of these protists. Our discovery of an
430 undescribed species, *Tritrichomonas casperi* (*Tc*), allowed us to compare this organism with
431 *Tritrichomonas musculis* (*Tmu*), which revealed unexpected metabolic diversity within this
432 genus. We show that succinate excretion as a fermentation waste product diverges between
433 *Tmu* and *Tc* metabolism, leading to markedly altered immune responses in the small intestine.
434 We also reveal that these protists rely on different carbohydrate sources in the gut, with *Tc*
435 functioning as a mucin-specialist and *Tmu* as a mucin-generalist that preferentially ferments
436 dietary MACs. Changing the composition of MACs in the diet shifts the competitive balance
437 between *Tmu* and bacteria, which alters host immunity. Our studies highlight the importance of
438 commensal protist metabolism in mediating diverse and complex interactions between diet,
439 intestinal immunity, and the microbiota.

440 A ubiquitous feature of previous studies on commensal tritrichomonads has been type 2
441 immunity in the small intestine resulting from succinate stimulation of tuft cells. Although

442 succinate may originate from multiple physiological sources during tritrichomonad colonization,
443 it has been attributed to commensal *Tritrichomonas* metabolism based on inferred evolutionary
444 conservation of fermentative pathways with the urogenital pathogen *T. foetus* (Muller et al.,
445 2012). Here, we report *Tc* as the first commensal tritrichomonad to robustly colonize the small
446 intestine yet not induce a type 2 immune response. Because succinate is critical for protists to
447 initiate type 2 immunity, we examined parabasalid metabolism in more detail. We first
448 sequenced both *Tmu* and *Tc* genomes to genetically reconstruct their core carbohydrate
449 metabolisms. As predicted, *Tmu* encodes the genes required to produce succinate, and we
450 measured high levels of succinate in axenic *Tmu* cultures and the cecal contents of *Tmu*-
451 colonized mice. In contrast, *Tc* colonized mice had low levels of cecal succinate, but surprisingly
452 *Tc* expressed genes to produce this metabolite and contained high levels of intracellular
453 succinate. We hypothesize that *Tc* converts intracellular succinate to other unidentified
454 metabolic byproducts which do not induce small intestinal type 2 immunity.
455 All parabasalids must maintain cellular redox balance to sustain anaerobic energy
456 production and cell growth. *Tmu*, *Tc*, and *T. foetus* all belong to the class *Tritrichomonadea* and
457 maintain redox balance through intracellular succinate production, while *T. vaginalis* belongs to
458 the class *Trichomonadea* and generates lactate for the same metabolic purpose. This
459 observation led us to identify a phylogenetic split between the parabasalid classes
460 *Trichomonadea* and *Tritrichomonadea*, in which the former generates lactate and the latter
461 generates succinate. This discovery aids the prediction of fermentative pathways in
462 parabasalids based only on the ITS sequence. We successfully used this new phylogenetic
463 information to predict that the human-associated commensal parabasalid *P. hominis* produces
464 lactate but not succinate. Because of this finding, we expect that *P. hominis* does not induce
465 type 2 immunity in humans, but this commensal may stimulate alternative host effects through
466 lactate excretion, such as epithelial stem cell proliferation or antigen sampling by immune cells
467 (Iraporda et al., 2015; Lee et al., 2018; Morita et al., 2019). The richness of parabasalid species

468 in the human microbiota remains poorly characterized as the microbiomes of many global
469 populations are grossly understudied. Consequently, we anticipate that sequencing datasets
470 acquired from more diverse human populations will identify new species of parabasalids, and
471 our phylogenetic-based predictive framework will be a powerful tool to predict the production of
472 immunomodulatory metabolites by these protists. It also bypasses technically challenging
473 methods such as isolating and culturing new protists. However, further work is required to refine
474 this predictive model. For example, the basis for succinate production without excretion in *Tc* is
475 still unknown and thus cannot be predicted from phylogenetic information.

476 Our studies generated several new tools and datasets for commensal tritrichomonads
477 which will eliminate critical barriers that have stymied mechanistic studies of these protists. The
478 complete genomes of *Tmu* and *Tc* combined with targeted metabolomics and multiple
479 transcriptomic datasets form a valuable foundation for future studies, but the seemingly simple
480 ability to grow these tritrichomonads in culture is an essential step for microbiological
481 investigations. Previous studies, including our own, isolated tritrichomonads from mice and
482 cultured these organisms to remove other microbes for experimental colonization of naïve
483 animals (Chudnovskiy et al., 2016; Howitt et al., 2016; Nadjsombati et al., 2018; Schneider et
484 al., 2018). However, these protists did not robustly grow in axenic *in vitro* culture. This basic
485 capability is particularly crucial for members of the microbiota because the complexity of their
486 natural ecosystem confounds the ability to link phenotypes to single members of the community.
487 In addition, the high degree of strain-level variation and potential for genetic drift make growth in
488 culture and the ability to freeze/thaw isolates invaluable for increasing experimental rigor.
489 Further, culture represents the first major hurdle for developing any microbe into a genetically
490 tractable model.

491 Commensal tritrichomonads are unaffected by colonization resistance, which our results
492 suggest is due to an ability to outcompete bacteria for their preferred nutritional niche. *Tc* readily
493 excludes the mucolytic bacteria *A. muciniphila* and *Bacteroidetes* spp., whereas these same

494 bacteria outcompete *Tmu* during dietary MAC deprivation. However, *Tmu* coexists with these
495 bacteria when inulin is the sole dietary MAC, even though *Tmu* cannot directly metabolize this
496 fiber. Many *Bacteroidetes* species can ferment both inulin and mucus glycans but prioritize fiber
497 over mucus (Desai et al., 2016; Lynch and Sonnenburg, 2012; Sonnenburg et al., 2010).
498 *Bacteroides thetaiotaomicron's* preference for fiber over mucus occurs via direct suppression of
499 mucus CAZymes by fiber-derived monosaccharides. An inulin-based diet may alleviate
500 competition for mucus, enabling *Tmu* to capitalize on this relatively open niche. Importantly,
501 *Tmu*'s flexible metabolic strategy appears well adapted to the dietary patterns of wild mice.
502 These rodents are opportunistic omnivores but preferentially consume plant-based foods such
503 as grains and seeds (Morris et al., 2012). Thus, while the types of plant polysaccharides may
504 fluctuate in the murine diet, their presence is relatively stable, which would allow *Tmu* a constant
505 supply of either dietary MACs or mucus derived glycans.
506 Commensal parabasalids are rare in the microbiotas of humans in industrialized
507 countries, despite extremely high prevalence throughout the animal kingdom (Brune, 2014;
508 Céza et al., 2015; Hampl et al., 2007; Malik et al., 2011). Human diets were historically high in
509 dietary MACs throughout evolution, but the Western diet contains far less of these key microbial
510 nutrients. This dietary shift, along with changes to sanitation and antibiotic usage, has been
511 associated with many consequences to health and microbiome diversity (Ferreyra et al., 2014;
512 Smits et al., 2017; Sonnenburg et al., 2016; Zinöcker and Lindseth, 2018), and our results
513 suggest that loss of commensal parabasalids may be another consequence of an industrialized
514 lifestyle. The absence of an entire phylum of microbes from the microbiota likely has wide-
515 ranging impacts on host health, particularly given the dramatic effects these protists have on
516 host intestinal immunity, the epithelium, and numerous diseases. Our results also reveal that
517 lack of colonization with certain commensal tritrichomonads is associated with decreased
518 microbiome diversity, suggesting a possible butterfly effect of downstream consequences to the
519 microbiome community. Furthermore, our data demonstrate that although fiber supplementation

520 rescues *Tmu* colonization, the types of dietary MACs present can drastically alter the host
521 response elicited by the protist. Thus, to accurately predict how colonization with individual
522 parabasalid species may impact human health, the interplay of microbial metabolism, trans-
523 kingdom interactions, and diet must be taken into consideration.
524

525 **Acknowledgements**

526 We thank members of the Howitt lab, John Boothroyd, Markus Lakemeyer, Rebecca Gellman,
527 and Fatima Enam for their helpful discussions and expertise. We also thank Dylan Maghini, Eli
528 Moss, Roshni Patel, and Sandra Kong for their NGS expertise. We thank John Perrino and Ruth
529 Yamawaki at the Stanford Cell Sciences Imaging Facility for expertise and help with sample
530 processing and scanning electron microscopy. We thank Amgen for kindly providing the *Gpr91*$^{-/-}$
531 mice. This work was supported by grants from the NIH (R01DK128292, K01DK113041,
532 R01AI14862302, R01AI14375702, 5 T32 AI07290, and T32HL120824), and a Jacob Churg
533 award to M.R.H.. E.R.G. is supported by the Stanford Pediatric IBD and Celiac Disease
534 Research Program and the Stanford Maternal & Child Health Research Institute.
535

536 **Author contributions**

537 E.R.G, S.Z., P.T.W., A.S.B., and M.R.H. designed the experiments. E.R.G., S.Z., P.T.W.,
538 C.M.M., J.A.L., F.K., S.K.H. performed experiments and contributed intellectual expertise.
539 A.M.S., J.L.S., A.S.B., provided intellectual expertise. E.R.G. and M.R.H. conceived the study
540 and wrote the manuscript, and all authors read and commented on the manuscript.
541

542 **Declaration of interests**

543 The authors declare no relevant competing interests.
544
545

546 **Figure legends**

547 **Figure 1. Identification of a novel gut protist in mice**

548 (A) FACS purification of the large *T. musculis* (*Tmu*) and small *T. casperi* (*Tc*) protists isolated
549 from a mouse cecum. FSC, forward scatter. SSC, side scatter. (B) SEM images of *Tmu* (left)
550 and *Tc* (right). UM: Undulating Membrane, RF: Recurrent Flagellum, AF: Anterior Flagella.
551 Scale bars are 2μm. (C) *Tmu* and *Tc* cell body lengths, measured by SEM. (D) Phylogram of
552 parabasalid protists based on ITS sequences. *Tmu* and *Tc* are marked with blue and red text,
553 respectively. (E) Tuft cell frequency measured by flow cytometry in the distal SI epithelium of
554 uncolonized (Ctrl) mice or those colonized with *Tmu* or *Tc* (F) Representative
555 immunofluorescence microscopy images of tuft cell hyperplasia in the distal SI epithelium of Ctrl
556 mice (left), *Tmu* colonized mice (middle), and *Tc* colonized mice (right). Tuft cells stained with
557 Dclk1, green. Epithelial cell membranes stained with E-cadherin, red. Nuclei stained with DAPI,
558 blue. Scale bars are 50μm. (G) Frequency of $GATA3^+$ $CD4^+$ T cells (Th2 cells) in the lamina
559 propria of the distal SI of mice colonized by each protist, measured by flow cytometry. Graphs
560 (C, E, G) depict mean. Error bars (C) depict SD. Each symbol represents an individual mouse
561 from 3 pooled experiments (E and G). ***$p<0.001$, ****$p<0.0001$, NS, not significant by Student's
562 t test.

563

564 **Figure 2. T Cell responses to *Tmu* and *Tc* differ in the small intestine but are similar in**
565 **the colon**

566 (A) Frequency of IFNγ and IL-17 producing $CD4^+$ T cells (Th1 and Th17 cells) in the distal SI
567 lamina propria of mice colonized by *Tc*. (B) Representative flow cytometry plots of the frequency
568 of IFNγ and IL-17 positivity in $CD4^+$ T cells isolated from the lamina propria of the distal SI. (C)
569 Frequency (top) and absolute abundance (bottom) of IFNγ and IL-17 positive $CD4^+$ T cells in the
570 colonic lamina propria. (D) Representative flow cytometry plots of the frequency of IFNγ and
571 IL17 positivity in colonic lamina propria $CD4^+$ T cells of *Tmu* and *Tc* colonized mice. (E and F)

572 Representative immunofluorescence microscopy images of *Tmu* (E) and *Tc* (F) in the colon.
573 Protists stained with anti-*Tmu* antibody, green. Epithelial cells stained with E-Cadherin, white.
574 Nuclei stained with DAPI, blue. Mucus layer stained with UEA1, red. Scale bars are 50μm.
575 Graphs depict mean. Each symbol represents an individual mouse from two (A) or three (C)
576 pooled experiments. *p<0.05, ***p<0.001, ****p<0.0001, NS, not significant by Student's t test.
577
578 **Figure 3. Metabolic differences in tritrichomonads underly divergent immune responses**
579 (A) Extracellular succinate concentration in the cecal contents of protist-colonized mice. (B, C)
580 Genome assemblies of *Tmu* (B) and *Tc* (C). Outermost rings show position (in Mbp), middle ring
581 shows genome assembly contigs, inner ring shows GC content in 10kb sliding windows. Total
582 genome size (in Mbp) is at the center of each circle. (D) Schematic of metabolic pathways in
583 parabasalid protists. The two fermentative pathways found in parabasalids are in boxes. Red
584 boxes surround pathways found in *Tc*, blue box surrounds the pathway found in *Tmu*. (E and F)
585 Gene expression levels (in transcripts per million (TPM)) in the cecum vs. distal SI for *Tmu* (E)
586 and *Tc* (F). Transcripts in the lactate and succinate fermentative pathways are labelled if
587 present. (G and H) Intracellular succinate (G) and lactate (H) measurements from purified *Tmu*
588 and *Tc* cell lysates. (I) Phylogenetic tree of parabasalids. Species in purple are confirmed
589 lactate producers, species in green are confirmed succinate producers. Asterisks signify new
590 metabolic confirmations in this study. Lines on the right indicate phylogenetic classes. Graphs
591 (A, G) depict mean with SD. **p<0.01, NS, not significant by Student's t test.
592
593 **Figure 4. *Tmu* and *Tc* occupy different nutritional niches within the microbiota**
594 (A) Abundance of *Tmu* and (B) *Tc* in the stool of mice fed diets with defined fiber compositions
595 for two weeks. Inulin and cellulose are the only fibers present in the defined chow. (C) 16S
596 rRNA amplicon sequencing in the stool of uncolonized (Ctrl) mice or mice colonized with *Tmu* or
597 *Tc* for 3 weeks. Data shown is average of 5 mice per group. (D) Linear Discriminant Analysis

598 scores showing bacterial microbiome composition changes associated with *Tc* colonization.
599 OTUs in green have higher relative abundance with *Tc* colonization, OTUs in red have lower
600 relative abundance with *Tc* colonization. (E) qPCR quantification of *A. muciniphila* relative
601 abundance in the stool of mice colonized with each protist. (F) Abundance (in TPM) of putative
602 mucus-utilization genes in *Tc* and *Tmu*. For putative mucolytic CAZymes the glycoside
603 hydrolase family (GH) is indicated in brackets. Graphs (A, B, E) depict mean, error bars depict
604 SD in (E). Each symbol represents an individual mouse from three pooled experiments.
605 **p<0.01, ***p<0.001, ****p<0.0001, NS, not significant by Mann-Whitney test.
606
607 **Figure 5. Dietary MAC deprivation causes *Tmu* to switch to a mucolytic metabolism**
608 (A) Representative images of *Tmu* in the colons of mice fed complex chow (left) and cellulose
609 chow (right) for two weeks. *Tmu* stained with anti-*Tmu* antibody, green. Mucus stained with
610 UEA1, red. Nuclei stained with DAPI, blue. Scale bar is 100μm. (B) Growth curves of *Tmu*
611 cultured *in vitro*, using the newly developed PBF medium, with maltose (blue) or mucus (green)
612 added as carbon sources, or with no defined carbon source added (grey). (C) Differential gene
613 expression from *Tmu* grown *in vitro* with either maltose or mucus as a carbon source. Green
614 data points indicate putative mucus-utilization genes with increased expression when grown in
615 the presence of mucus. GH families for putative mucolytic CAZymes are labelled. Dashed lines
616 delineate the fold change cutoff (1.5-fold). (D) *Tmu* abundance in the stool of mice fed defined
617 chow or cellulose chow for two weeks, with or without antibiotics. Antibiotics used are
618 Vancomycin, V; Neomycin, N; Ampicillin, A. (E) *Tmu* abundance in the cecal contents of mice
619 fed cellulose chow for two weeks with different antibiotic treatments. (F) 16S rRNA amplicon
620 sequencing of *Tmu*-colonized mice fed cellulose for two weeks with different antibiotic
621 treatments. (G) Relative abundance of known mucolytic bacteria in mice from each group in (F).
622 LD, limit of detection. Graphs (B, D, E, G) are plotted as mean, error bars depict SD in (B). Each

623 symbol represents an individual mouse from three pooled experiments (D and E). **p<0.01,
624 ****p<0.0001, NS, not significant by Mann-Whitney test.
625
626 **Figure 6. Diet-protist interactions shape the host immune response**
627 (A) *In vitro* growth curve of *Tmu* cultured with maltose (blue) or inulin (purple) added as carbon
628 sources, or with no defined carbon source added (grey). (B) Representative images of *Tmu* in
629 mice fed complex chow (varied dietary MAC composition), defined chow (inulin and cellulose),
630 or cellulose chow. *Tmu* stained with anti-*Tmu* antibody, green. Mucus stained with UEA1, red.
631 Nuclei stained with DAPI, blue. Scale bar is 50μm. (C) Relative abundance of *Bacteroidetes*
632 bacteria in the stool of mice colonized by *Tmu* (left) and *Tc* (right), with the fermentable fiber
633 inulin or the non-fermentable fiber cellulose as the only fiber sources in the diet. (D) Maximum
634 *Tmu* culture density when grown *in vitro* with different dietary MACs added as carbon sources to
635 PBF medium. All statistical comparisons are relative to culture with no defined carbon source
636 added. (E) Differential expression of *Tmu* grown *in vitro* with either maltose or arabinoxylan as a
637 carbon source. Cyan data points represent upregulated CAZymes with potential activity towards
638 arabinoxylan. Dashed lines delineate the fold change cutoff (1.5-fold). (F) Tuft cell frequency in
639 the distal SI epithelium of mice fed complex chow (varied dietary MACs) and defined chow
640 (inulin and cellulose). (G) *Tmu* abundance in the distal SI of mice fed complex chow and defined
641 chow. Data is plotted as mean with SD (A and D). Each symbol represents an individual mouse
642 from two (C) or three (F, G) pooled experiments. *p<0.05, **p<0.01, ***p<0.001, ****p<0.0001,
643 NS, not significant by Mann-Whitney test (G) or Student's t test (C, F).
644
645
646
647
648

649 **STAR METHODS**

650

651 **RESOURCE AVAILABILITY**

652 **Lead contact**

653 Further information and requests for resources and reagents may be directed to and will be
654 fulfilled by the lead contact, Michael Howitt (mhowitt@stanford.edu).

655 **Materials availability**

656 Mouse and microbial strains used in this study will be made available upon request addressed
657 to the lead contact.

658

659 **Animals**

660 C57BL/6 mice were purchased from Jackson Laboratory. Mice from Jackson Laboratory are
661 protist negative, as verified by PCR on the stool and examination of cecal contents. *Gpr91*$^{-/-}$
662 mice were generously provided by Amgen under a materials transfer agreement. All mice were
663 used at 6-12 weeks of age. Experiments were performed using age and gender matched
664 groups. All animal procedures used in this study were approved by the Institutional Animal Care
665 and Use Committee (IACUC) at Stanford School of Medicine.

666 Mice were housed in individually ventilated cage systems and maintained at specific
667 pathogen free (SPF) health status. Colonies of protist-negative and protist-colonized mice were
668 maintained and handled separately. Protist colonization status was routinely verified by PCR on
669 stool and examination of cecal contents by light microscopy. Cage bottoms were covered with
670 autoclaved bedding and enrichment material. Mice were handled within HEPA filtered air
671 exchange stations, and all surfaces and tools were sanitized using Virkon™ S disinfectant
672 before and after handling. All cage changes were performed by lab staff, who were required to
673 wear personal protection equipment (lab coats, gloves, disposable sleeves) to handle mice used
674 in this study.

675 Custom diets for *in vivo* fiber experiments were obtained from Research Diets, Inc. The
676 diets were the same as those used previously (Schneider et al., 2018), with diet IDs D11112201
677 (Defined chow with cellulose and inulin), D11112229 (no fiber), D17030102 (cellulose),
678 D11112226 (inulin). For antibiotic treatment experiments, mice were given antibiotics in the
679 drinking water, which was changed every 3 days. Antibiotics and concentrations were:
680 vancomycin (0.5g/mL), neomycin (1g/mL), ampicillin (1g/mL). For succinate treatment, disodium
681 succinate (100mM) was added to the drinking water and changed every 3 days.
682
683 **Method details**
684 Identification of protists in mouse stool
685 Mice at Stanford University animal facilities were screened for commensal protists by extracting
686 DNA from stool using the Powersoil Pro Kit (Qiagen) according to manufacturer instructions.
687 Samples were then used as input for PCR using pan-parabasalid primers (forward: 5'-
688 CCACGGGTAGCAGCA-3', reverse: 5'-GGCAGGGACGTATTCAA-3'). These primers generate
689 an approximately 1.1kb amplicon of the parabasalid internally transcribed spacer (ITS)
690 sequence, which was sequenced by Sanger Sequencing for phylogenetic classification.
691 Phylograms were generated using phylogeny.fr (Lemoine et al., 2019).
692 Isolation of *Tritrichomonas spp.* from mice
693 Protists were purified as described previously (Howitt et al., 2016), with modifications. Briefly,
694 cecal contents were harvested from WT C57BL/6 mice and passed over a 40μm strainer.
695 Contents were then washed three times in PBS and purified at the interface of a 40%/80%
696 Percoll (GE healthcare) gradient, after centrifugation at 1000xg for 10minutes with no brake.
697 The number of viable protists was quantified using a hemocytometer, and $1x10^6$ trophozoites
698 were inoculated per mL of PBF growth medium (recipe below). The PBF medium was
699 supplemented with 1x Penicillin/Streptomycin (Caisson Labs), 2.5μg/mL Amphotericin B (Sigma

700 Aldrich), 100µg/mL Vancomycin (Alfa Aesar), 12.5µg/mL Chloramphenicol (Sigma). Protists
701 were then cultured overnight in an anaerobic chamber (Coy Labs) at 37˚C.
702 Colonization of mice with protists
703 Mice were colonized with commensal parabasalid protists as described previously (Howitt et al.,
704 2016) with slight modifications. Briefly, protists were resuspended in PBS and mice were
705 colonized with $1x10^5$ protists per mouse by oral feeding. Colonization was verified after 7 days
706 by qPCR on the stool using *Tmu* or *Tc* specific primers. For *Tc* colonization of mice, protists
707 were isolated directly from mouse ceca one day prior to colonization. For *Tmu* colonization of
708 mice, protists were cultured *in vitro* for no more than 20 passages prior to colonization of mice.
709 Scanning Electron Microscopy (SEM)
710 SEM was performed on *Tmu* and *Tc* as described previously (Howitt et al., 2016). Briefly,
711 protists were isolated from the ceca of SPF mice as described above and adhered to poly-lysine
712 coated coverslips. Samples were then fixed in 2.5% glutaraldehyde in 0.1M cacodylate pH 7.2.
713 Samples were then rinsed and post-fixed for 30min in 1% OsO_4 in 0.1M cacodylate buffer and
714 dehydrated in a graded series of ethanol prior to critical point drying with liquid CO_2. Protists
715 were then sputter-coated with 5nm platinum and examined with a Zeiss Sigma scanning
716 electron microscope.
717 High molecular weight DNA extraction and Nanopore Sequencing
718 To obtain pure protist DNA for genome sequencing, *Tc*-colonized mice were treated with an
719 antibiotic and antifungal cocktail in the drinking water (0.5g/L Vancomycin, 1g/L Neomycin, 1g/L
720 Ampicillin, 0.2g/L Amphotericin B) for 6 days. *Tc* was then purified from the cecal contents as
721 described above, with the modification of two rounds of Percoll purification, instead of one. For
722 *Tmu*, protists were instead axenically cultured. High molecular weight DNA from each protist
723 was then isolated by gently resuspending pelleted protists in lysis buffer (PBS+0.5% sodium
724 dodecyl sulfate), using a wide-bore pipet tip. Lysed cells were transferred to DNA LoBind tubes
725 (Eppendorf) and incubated with Monarch RNase A (NEB) for 2 hours at 37˚C. Next, Proteinase

726 K (Qiagen) was added, and samples were incubated for 2 hours at 50˚C. Nucleic acid was then
727 isolated using two rounds of extraction with Phenol:Chloroform:Isoamyl alcohol (Sigma). To
728 avoid pipetting during transfer steps, vacuum grease (Dow Corning) was added as a phase-lock
729 gel. Protein contaminants were then precipitated using 2M Ammonium Acetate, and then DNA
730 was precipitated overnight in ethanol. Next, DNA was pelleted by centrifugation at 8000xg, and
731 DNA pellets were washed three times with 70% ethanol. DNA was then resuspended in water
732 and used for library preparation and sequencing using the Nanopore Ligation Sequencing Kit
733 and Minion Flow Cell (Oxford Nanopore).

734 Genome assembly and annotation

735 Genome assemblies for both *T. casperi* and *T. musculis* were constructed using Flye
736 (Kolmogorov et al., 2019), v. 2.9-b1768 with default parameters. Short read libraries were then
737 mapped against the genome assemblies with Bowtie2 (Langmead and Salzberg, 2012), v. 2.4.4
738 and resulting alignments were used for assembly polishing with pilon (Walker et al., 2014).
739 Genes were predicted with MetaEuk (Karin et al., 2020), v. 5.34c21f2 with Uniref90 as the
740 reference protein dataset. Genome completeness was assessed with BUSCO (Manni et al.,
741 2021), v5.0.0 in protein mode with Eukaryota ODB10 lineage marker gene set. Genome
742 diagrams were generated using DNAPlotter (Carver et al., 2009), v. 18.2.0.

743 RNA-Sequencing

744 RNA-Sequencing was performed on *Tmu* and *Tc in vivo* by first isolating the luminal contents
745 from the distal small intestine and cecum of 3 mice per group. Contents were strained over
746 40µm filters, then washed with ice-cold PBS to remove debris. To minimize potential for sample
747 processing to affect transcriptomes, samples were then immediately resuspended in Qiazol
748 (Qiagen). RNA was purified using the Direct-zol RNA Miniprep kit (Zymo Research). RNA-Seq
749 libraries were then generated using the KAPA Stranded RNA-Seq kit with poly-dT enrichment of
750 mRNA transcripts, and libraries were sequenced on an Illumina HiSeq instrument.

751 Transcriptomics on the *in vitro* grown *Tmu* samples was performed on protists grown for
752 3 days in the condition of interest. Cultures (3 biological replicates per condition) were pelleted
753 at 700xg for 5min at 4˚, then resuspended in Qiazol. RNA was then isolated using the Direct-zol
754 RNA Miniprep kit (Zymo Research), as above. Library preparation and sequencing was
755 performed at Azenta Life Sciences (South Plainfield, NJ). Libraries were constructed using the
756 TruSeq Stranded mRNA kit (Illumina), with poly-dT enrichment of mRNA transcripts. Samples
757 were sequenced on a HiSeq instrument (Illumina).
758 Analysis of all transcriptomics datasets was performed using alignment-based analysis,
759 using the newly sequenced *Tmu* and *Tc* genomes. Briefly, Illumina adapters were trimmed and
760 low-quality sequence was removed using Trimmomatic (Bolger et al., 2014). Reads were then
761 aligned to the respective genome using Burrows Wheeler Aligner (Li and Durbin, 2009).
762 Samtools (Danecek et al., 2021) was used to convert corresponding files to binary alignment
763 and map (bam) files and sort the reads by position. Next, featureCounts (Liao et al., 2014) was
764 used to quantify read depth of each genome feature. Differential expression analysis was
765 performed using DESeq2 (Love et al., 2014).
766 <u>Protist enumeration</u>
767 Enumeration of protists from the small intestinal tissue was performed as described previously
768 (Howitt et al., 2016), with modifications. Briefly, the distal 10cm of small intestine was removed
769 and flushed with ice-cold sterile PBS using a 19-gauge feeding needle. The contents were then
770 pelleted and the supernatant was aspirated. Genomic DNA was isolated using the Powersoil
771 Pro Kit (Qiagen) according to manufacturer instructions. To detect and enumerate protists,
772 quantitative PCR (qPCR) was performed using PowerUp SYBR Green Master Mix (Applied
773 Biosystems). For *T. musculis*, the following primers specific to the 28S rRNA gene were used:
774 5'-GCTTTTGCAAGCTAGGTCCC-3'and 5'- TTTCTGATGGGGCGTACCAC-3' (Howitt et al.,
775 2016). For *T. casperi* detection, primers were designed that specifically recognized this protist:
776 5'-AGGTTACTGAATCATACATGCGT-3' and 5'-GCAGGAGTTGCTTTCATTGTG-3'. qPCRs

777 were run on a QuantStudio 3 Real Time PCR instrument (Thermo Fisher). To convert qPCR
778 values into protist numbers, protists were isolated and counted using a hemocytometer before
779 extracting genomic DNA and analyzing a dilution series by qPCR. These results were used to
780 create a standard curve, and regression analysis was used to convert Ct values to protist
781 numbers, as has been described previously (Chudnovskiy et al., 2016; Howitt et al., 2016).
782 Quantification of protists in the stool was performed similarly. Stool pellets were
783 collected from mice and weighed. A fraction of the stool was dried and used to calculate the
784 water content of the stool, while the rest was used for DNA extraction. Quantification was
785 performed using the same qPCR primers as above. Protists were quantified in the cecum by
786 weighing the cecal luminal contents, then resuspending in PBS. Live trophozoites were then
787 counted using a hemocytometer and normalized to cecal weight.
788 Isolation of Epithelial Cells for Flow Cytometry
789 For epithelial flow cytometry for tuft cell quantification, mice were colonized by protists by
790 vertical transmission. Ileal epithelial cells were isolated as described previously (Howitt et al.,
791 2016). Briefly, the terminal 10cm of the small intestine was removed and trimmed of fat. Luminal
792 contents were gently flushed with 10mL of ice-cold PBS, then the tissue was opened
793 longitudinally. Peyer's Patches were removed and the tissue was incubated on ice in PBS, 5mM
794 HEPES pH 7.4, 2% heat-inactivated fetal bovine serum (iFBS), 1mM DTT. Tissue was then
795 transferred to pre-warmed PBS, 5mM HEPES, 2% iFBS, 5mM EDTA and shaken at 200rpm for
796 15 minutes at 37˚, followed by vigorous shaking. This was repeated and epithelial cells from
797 both fractions were combined and washed with PBS. Tissue was then digested in DMEM
798 containing 10% iFBS, 0.5U/mL Dispase II (StemCell Technologies), 50µg/mL DNase (Roche)
799 for 10 minutes at 37˚C. The cells were then filtered over 40µm strainers and washed with PBS,
800 2% iFBS, 1mM EDTA. Cells were then incubated for 10 minutes with anti-CD16/CD32 (clone
801 93, Biolegend) and then stained with the following antibodies: PacBlue-conjugated anti-CD45
802 (clone 30-F11, Biolegend), PE/Cy7-conjugated anti-EpCam (clone G8.8, Biolegend), and

803 Alex647-conjugated anti-SiglecF (clone E50-2440, BD Biosciences). Cell viability was assessed
804 by propidium iodide staining (Biolegend). Cells were then analyzed on a BD FACSCanto II.
805 Lamina propria cell isolation and flow cytometry
806 For lamina propria flow cytometry for immune cell analysis, mice were colonized by protists by
807 vertical transmission. The distal 10cm of small intestine, or the entire colon, were collected and
808 epithelial cells were removed as described above. The remaining tissue was then minced and
809 digested in RPMI 10% iFBS, 0.1 units/mL Dispase II (StemCell Technologies), 50µg/mL DNase
810 (Roche), collagenase A (Roche) (0.25mg/mL for ilea, 0.5mg/mL for colons). Tissue was
811 digested for 30 minutes followed by a second digestion for 40 minutes. Digested tissue was
812 passed through a 40µm strainer, and the cells were counted using a Cellometer Auto T4
813 (Nexcelom Bioscience). For cytokine measurements, cells were stimulated in RPMI
814 supplemented with 10% iFBS, Pen/Strep, PMA, Ionomycin, and GolgiPlug. Cells were
815 incubated at 37˚ for 4 hours to allow stimulation to occur before being harvested. Cells were
816 then incubated with anti-CD16/32 (clone 92, Biolegend) before surface staining with PacBlue-
817 conjugated anti-CD45 (clone 30-F11, Biolegend), FITC-conjugated anti-CD4 (clone GK1.5,
818 Biolegend), and PerCP/Cy5.5-conjugated anti-CD3 (clone 17A2, Biolegend). Cells were then
819 stained with the viability dye Zombie-NIR (Biolegend) according to manufacturer instructions
820 prior to fixation with the Foxp3 Transcription factor staining buffer set (eBioscience). Fixed cells
821 were permeabilized and stained with PE-conjugated anti-IL17 (clone 9B10, Biolegend) and
822 APC-conjugated anti-IFNγ (clone XMG1.2, eBioscience). Cells were then analyzed on a BD
823 FACSCanto II.
824 Tissue preparation and staining for immunofluorescence
825 Tissue sections of interest were removed and fixed in methacarn fixative (Fisher Scientific) for
826 48 hours. Tissue was then washed three times in 100% ethanol, followed by three washes in
827 Histo-Clear II (Electron Microscopy Sciences). Fixed tissue was embedded in paraffin wax prior
828 to sectioning (4µm) using a microtome. For immunofluorescence, tissue was first deparaffinized

829 as has been described previously (Earle et al., 2015), then blocked with blocking buffer (PBS
830 supplemented with 3% BSA, 0.1% Saponin, 2% goat serum). Sections were then stained with
831 the anti-*Tmu* antibody (generated by Rockland Scientific) and anti-E Cadherin (clone 36/E)
832 overnight. After 3 washes in PBS, sections were stained with secondary antibodies fluorescently
833 conjugated to Alexa488 (*Tmu*) and Alexa660 (E Cadherin). DAPI (Sigma Aldrich) and
834 rhodamine-conjugated Ulex Europaeus Agglutinin I (Vector Laboratories) were added during the
835 secondary staining step as well. After 3 PBS washes, tissue was mounted with Vectashield
836 (Vector Labs) and imaged on a Zeiss LSM 700 confocal microscope.

837 Metabolite measurements

838 For intracellular metabolite analysis, mice were treated with an antibiotic cocktail in the drinking
839 water (0.5g/L Vancomycin, 1g/L Neomycin, 1g/L Ampicillin, 0.2g/L Amphotericin B) for 6 days.
840 Protists were then isolated as described above and lysed in 1mL 80% methanol. Cellular debris
841 was removed through centrifugation, followed by filtration using 0.22μm filters, snap frozen in
842 liquid nitrogen, and stored at -80˚. Prior to liquid chromatography mass spectrometry (LC/MS)
843 analysis, intracellular extracts (800 μL) were dried in a vacuum concentrator at room
844 temperature for approximately 4 hours then resuspended in 50 μL of HPLC-grade water spiked
845 with ^{13}C-labeled metabolites as an internal standard.

846 For metabolite measurements from cecal supernatants, cecal contents were squeezed
847 into tubes and weighed, prior to gentle resuspension in sterile saline solution (0.15M NaCl).
848 Samples were then pelleted at 500xg for 5min at 4˚, and supernatants were transferred to clean
849 tubes. Samples were then pelleted at 2000xg for 10min at 4˚, and then supernatants were
850 filtered over 0.22μm filters, snap frozen in liquid nitrogen, and stored at -80˚. Prior to LC/MS
851 analysis, cecal extracts were diluted in HPLC-grade water spiked with ^{13}C-labeled metabolites
852 as an internal standard.

853 For organic acid measurements, samples (5 μL) were run in reverse phase on a 2.1 mm
854 x 150 mm Waters Acquity UPLC BEH C18 column with 1.7 μm packing. The column was fitted

855 with a Vanguard pre-column of the same composition. Analytes were separated on an Agilent
856 1290 Infinity II UPLC (binary pumps) and detected using an Agilent 6545 LC/MS Quadrupole
857 Time-of-Flight (qTOF) instrument equipped with a dual jet stream electrospray ionization source
858 (ESI) operating under extended dynamic range (EDR 1700 m/z) in the negative (ESI-) ionization
859 mode. The mobile phase solvents consisted of 20 mM ammonium formate pH 2.9 (A) and
860 acetonitrile (B). The separation began with 99.5% A and 0.5% B for 4 min at 0.4 mL/min, then B
861 was increased to 99.5% at 0.5 mL/min and held for 1.5 min, at which time the flow rate was
862 increased to 0.8 mL/min. At 11.5 min, solvent B was reduced to 0.5% and the flow rate was
863 reduced to 0.5 mL/min for 2.5 min, at which time it was further reduced to 0.4 mL/min. The
864 separation ended at 14 min. Specific ion source parameters included: Drying gas temperature
865 was 150˚C at 12L/min, sheath gas temperature was 325˚C at 12 L/min, Nebulizer was at 45
866 psig, capillary voltage was 2000 V, nozzle voltage was 0V, fragmentor voltage was 90 V,
867 skimmer voltage was at 35 V, octopole RF was 750V. For quantitation purposes, standard
868 curves of all analytes were prepared in HPLC water spiked with ^{13}C-labeled metabolites as an
869 internal standard. Metabolite levels were determined by manually integrating the area under
870 each chromatographic peak and their concentrations in the samples determined by interpolating
871 the peak area for each compound on the corresponding standard curve.
872 For short chain fatty acid measurements, samples were prepared as described above.
873 Short chain fatty acids were identified as described previously (Meshulam-Simon et al., 2007),
874 using HPLC-UV with an Aminex HPX-87H column (Bio-Rad, Hercules, CA).
875 Dietary fiber experiments
876 For experiments involving manipulation of dietary fiber, mice (fed normal complex chow) were
877 colonized by $1x10^5$ protists between 4-6 weeks of age. Ten days later, the diets were changed
878 to chows with defined fiber compositions. Stool was collected for protist quantification two
879 weeks later, and mice were euthanized for collection of tissue for additional analyses. For
880 experiments involving manipulation of dietary fiber and antibiotic treatment, mice were colonized

881 by protists as above. Ten days later, mice were started on the indicated antibiotic treatment,
882 followed by diet switch three days after the start of antibiotics.

883 16S Bacterial Profiling

884 For 16S bacterial profiling, mice were colonized by $1x10^5$ protists between 4-6 weeks of age,
885 and stool was collected 3 weeks later for microbiome analysis. DNA was extracted using the
886 Powersoil Pro Kit (Qiagen). The DNA samples were prepared for targeted sequencing at Zymo
887 Research (Irvine, CA). Libraries were made using the *Quick*-16S NGS Library Prep Kit using
888 Primer Set V3-V4 (Zymo Research, Irvine, CA). Samples were sequenced on an Illumina MiSeq
889 with a v3 reagent kit. Unique amplicon sequences were inferred from raw reads using the
890 Dada2 pipeline (Callahan et al., 2016). Chimeric sequences were removed, and taxonomy
891 assignment was performed using Uclust from Qiime2 (Bolyen et al., 2019). Taxonomy was
892 assigned with the Zymo Research 16S Database. Alpha-diversity and composition analyses
893 were performed with Qiime. Taxonomy abundance differences between groups were identified
894 by LEfSe (Segata et al., 2011).

895 Absolute abundance quantification was performed using qPCR. A standard curve was
896 made with plasmid DNA containing one copy of the 16S gene, prepared in 10-fold serial
897 dilutions. The primers used were the same as those used in targeted library preparation. The
898 equation generated by the plasmid DNA standard curve was used to calculate the number of
899 gene copies in the reaction for each sample. The PCR input volume was used to calculate the
900 number of gene copies in each DNA sample. The number of genome copies per microliter of
901 DNA in each sample was calculated by dividing the gene copy number by an assumed number
902 of gene copies per genome. The value used for 16S copies is 4. The amount of DNA per
903 microliter of sample was calculated using an assumed genome size of $4.64x10^6$bp, the genome
904 size of *Escherichia coli*. The mass of the stool sample used for DNA extraction was then used to
905 calculate the number of genome copies per milligram of stool.

906 Bacterial relative abundance measurements by qPCR

907 *Akkermansia muciniphila* and *Bacteroidetes* quantification was performed using DNA isolated
908 from stool as described above. Relative abundance of bacterial groups were then quantified
909 using the following primers: *Akkermansia muciniphila* 5'-CAGCACGTGAAGGTGGGGAC-3', 5'-
910 CCTTGCGGTTGGCTTCAGAT-3' (Schneeberger et al., 2015). *Bacteroidetes* 5'-
911 GTTTAATTCGATGATACGCGAG-3', 5'-TTAASCCGACACCTCACGG-3' (Yang et al., 2015).
912 Universal 16S 5'-AAACTCAAAKGAATTGACGG-3', 5'-CTCACRRCACGAGCTGAC-3' (Yang et
913 al., 2015). qPCRs were performed using PowerUp SYBR Green Master Mix (Applied
914 Biosystems) on a QuantStudio 3 Real-Time PCR machine (Thermo Fisher). Ct values for
915 bacterial groups of interest were then normalized to total 16S for relative abundance analysis.
916 Quantification and Statistical Analysis
917 Groups were compared using Prism v9 software (GraphPad) using the two-tailed unpaired
918 Student's t test or Mann-Whitney test where appropriate. Differences were considered
919 statistically significant when $p \leq 0.05$.
920
921
922
923
924
925
926
927
928
929
930
931
932

933 **References**

934 Atarashi, K., Tanoue, T., Ando, M., Kamada, N., Nagano, Y., Narushima, S., Suda, W., Imaoka,
935 A., Setoyama, H., Nagamori, T., Ishikawa, E., Shima, T., Hara, T., Kado, S., Jinnohara,
936 T., Ohno, H., Kondo, T., Toyooka, K., Watanabe, E., Yokoyama, S., Tokoro, S., Mori, H.,
937 Noguchi, Y., Morita, H., Ivanov, I.I., Sugiyama, T., Núñez, G., Camp, J.G., Hattori, M.,
938 Umesaki, Y., Honda, K., 2015. Th17 Cell Induction by Adhesion of Microbes to Intestinal
939 Epithelial Cells. Cell 163, 367–380. https://doi.org/10.1016/j.cell.2015.08.058

940 Atarashi, K., Tanoue, T., Oshima, K., Suda, W., Nagano, Y., Nishikawa, H., Fukuda, S., Saito,
941 T., Narushima, S., Hase, K., Kim, S., Fritz, J.V., Wilmes, P., Ueha, S., Matsushima, K.,
942 Ohno, H., Olle, B., Sakaguchi, S., Taniguchi, T., Morita, H., Hattori, M., Honda, K., 2013.
943 Treg induction by a rationally selected mixture of Clostridia strains from the human
944 microbiota. Nature 500, 232–236. https://doi.org/10.1038/nature12331

945 Bae, M., Cassilly, C.D., Liu, X., Park, S.-M., Tusi, B.K., Chen, X., Kwon, J., Filipčík, P., Bolze,
946 A.S., Liu, Z., Vlamakis, H., Graham, D.B., Buhrlage, S.J., Xavier, R.J., Clardy, J., 2022.
947 Akkermansia muciniphila phospholipid induces homeostatic immune responses. Nature
948 1–6. https://doi.org/10.1038/s41586-022-04985-7

949 Barratt, J., Gough, R., Stark, D., Ellis, J., 2016. Bulky Trichomonad Genomes: Encoding a
950 Swiss Army Knife. Trends Parasitol. 32, 783–797.
951 https://doi.org/10.1016/j.pt.2016.05.014

952 Belkaid, Y., Hand, T.W., 2014. Role of the Microbiota in Immunity and Inflammation. Cell 157,
953 121–141. https://doi.org/10.1016/j.cell.2014.03.011

954 Bellali, S., Lagier, J.-C., Million, M., Anani, H., Haddad, G., Francis, R., Yimagou, E.K.,
955 Khelaifia, S., Levasseur, A., Raoult, D., Khalil, J.B., 2021. Running after ghosts: are
956 dead bacteria the dark matter of the human gut microbiota? Gut Microbes 13, 1–12.
957 https://doi.org/10.1080/19490976.2021.1897208

958 Billy, V., Lhotská, Z., Jirků, M., Kadlecová, O., Frgelecová, L., Parfrey, L.W., Pomajbíková, K.J.,
959 2021. Blastocystis Colonization Alters the Gut Microbiome and, in Some Cases,
960 Promotes Faster Recovery From Induced Colitis. Front. Microbiol. 12, 641483.
961 https://doi.org/10.3389/fmicb.2021.641483
962 Bolger, A.M., Lohse, M., Usadel, B., 2014. Trimmomatic: a flexible trimmer for Illumina
963 sequence data. Bioinformatics 30, 2114–2120.
964 https://doi.org/10.1093/bioinformatics/btu170
965 Bolyen, E., Rideout, J.R., Dillon, M.R., Bokulich, N.A., Abnet, C.C., Al-Ghalith, G.A., Alexander,
966 H., Alm, E.J., Arumugam, M., Asnicar, F., Bai, Y., Bisanz, J.E., Bittinger, K., Brejnrod, A.,
967 Brislawn, C.J., Brown, C.T., Callahan, B.J., Caraballo-Rodríguez, A.M., Chase, J., Cope,
968 E.K., Silva, R.D., Diener, C., Dorrestein, P.C., Douglas, G.M., Durall, D.M., Duvallet, C.,
969 Edwardson, C.F., Ernst, M., Estaki, M., Fouquier, J., Gauglitz, J.M., Gibbons, S.M.,
970 Gibson, D.L., Gonzalez, A., Gorlick, K., Guo, J., Hillmann, B., Holmes, S., Holste, H.,
971 Huttenhower, C., Huttley, G.A., Janssen, S., Jarmusch, A.K., Jiang, L., Kaehler, B.D.,
972 Kang, K.B., Keefe, C.R., Keim, P., Kelley, S.T., Knights, D., Koester, I., Kosciolek, T.,
973 Kreps, J., Langille, M.G.I., Lee, J., Ley, R., Liu, Y.-X., Loftfield, E., Lozupone, C., Maher,
974 M., Marotz, C., Martin, B.D., McDonald, D., McIver, L.J., Melnik, A.V., Metcalf, J.L.,
975 Morgan, S.C., Morton, J.T., Naimey, A.T., Navas-Molina, J.A., Nothias, L.F., Orchanian,
976 S.B., Pearson, T., Peoples, S.L., Petras, D., Preuss, M.L., Pruesse, E., Rasmussen,
977 L.B., Rivers, A., Robeson, M.S., Rosenthal, P., Segata, N., Shaffer, M., Shiffer, A.,
978 Sinha, R., Song, S.J., Spear, J.R., Swafford, A.D., Thompson, L.R., Torres, P.J., Trinh,
979 P., Tripathi, A., Turnbaugh, P.J., Ul-Hasan, S., Hooft, J.J.J. van der, Vargas, F.,
980 Vázquez-Baeza, Y., Vogtmann, E., Hippel, M. von, Walters, W., Wan, Y., Wang, M.,
981 Warren, J., Weber, K.C., Williamson, C.H.D., Willis, A.D., Xu, Z.Z., Zaneveld, J.R.,
982 Zhang, Y., Zhu, Q., Knight, R., Caporaso, J.G., 2019. Reproducible, interactive, scalable

983 and extensible microbiome data science using QIIME 2. Nat. Biotechnol. 37, 852–857.
984 https://doi.org/10.1038/s41587-019-0209-9
985 Brune, A., 2014. Symbiotic digestion of lignocellulose in termite guts. Nat. Rev. Microbiol. 12,
986 168–180. https://doi.org/10.1038/nrmicro3182
987 Callahan, B.J., McMurdie, P.J., Rosen, M.J., Han, A.W., Johnson, A.J.A., Holmes, S.P., 2016.
988 DADA2: High resolution sample inference from Illumina amplicon data. Nat. Methods 13,
989 581–583. https://doi.org/10.1038/nmeth.3869
990 Carlton, J.M., Hirt, R.P., Silva, J.C., Delcher, A.L., Schatz, M., Zhao, Q., Wortman, J.R., Bidwell,
991 S.L., Alsmark, U.C.M., Besteiro, S., Sicheritz-Ponten, T., Noel, C.J., Dacks, J.B., Foster,
992 P.G., Simillion, C., Peer, Y.V.D., Miranda-Saavedra, D., Barton, G.J., Westrop, G.D.,
993 Müller, S., Dessi, D., Fiori, P.L., Ren, Q., Paulsen, I., Zhang, H., Bastida-Corcuera, F.D.,
994 Simoes-Barbosa, A., Brown, M.T., Hayes, R.D., Mukherjee, M., Okumura, C.Y.,
995 Schneider, R., Smith, A.J., Vanacova, S., Villalvazo, M., Haas, B.J., Pertea, M.,
996 Feldblyum, T.V., Utterback, T.R., Shu, C.L., Osoegawa, K., Jong, P.J.D., Hrdy, I.,
997 Horvathova, L., Zubacova, Z., Dolezal, P., Malik, S.B., Logsdon, J.M., Henze, K., Gupta,
998 A., Wang, C.C., Dunne, R.L., Upcroft, J.A., Upcroft, P., White, O., Salzberg, S.L., Tang,
999 P., Chiu, C.H., Lee, Y.S., Embley, T.M., Coombs, G.H., Mottram, J.C., Tachezy, J.,
1000 Fraser-Liggett, C.M., Johnson, P.J., 2007. Draft genome sequence of the sexually
1001 transmitted pathogen Trichomonas vaginalis. Science 315, 207–212.
1002 https://doi.org/10.1126/science.1132894
1003 Carver, T., Thomson, N., Bleasby, A., Berriman, M., Parkhill, J., 2009. DNAPlotter: circular and
1004 linear interactive genome visualization. Bioinformatics 25, 119–120.
1005 https://doi.org/10.1093/bioinformatics/btn578
1006 Cepicka, I., Hampl, V., Kulda, J., 2010. Critical Taxonomic Revision of Parabasalids with
1007 Description of one New Genus and three New Species. Protist 161, 400–433.
1008 https://doi.org/10.1016/j.protis.2009.11.005

1009 Céza, V., Pánek, T., Smejkalová, P., Čepička, I., 2015. Molecular and morphological diversity of
1010 the genus Hypotrichomonas (Parabasalia: Hypotrichomonadida), with descriptions of six
1011 new species. Eur. J. Protistol. 51, 158–172. https://doi.org/10.1016/j.ejop.2015.02.003
1012 Chu, H., Mazmanian, S.K., 2013. Innate immune recognition of the microbiota promotes host-
1013 microbial symbiosis. Nat. Immunol. 14, 668–675. https://doi.org/10.1038/ni.2635
1014 Chudnovskiy, A., Mortha, A., Kana, V., Belkaid, Y., Grigg, M.E., Correspondence, M.M., 2016.
1015 Host-Protozoan Interactions Protect from Mucosal Infections through Activation of the
1016 Inflammasome. Cell 167, 444-456.e14. https://doi.org/10.1016/j.cell.2016.08.076
1017 Clemente, J.C., Ursell, L.K., Parfrey, L.W., Knight, R., 2012. The Impact of the Gut Microbiota
1018 on Human Health: An Integrative View. Cell 148, 1258–1270.
1019 https://doi.org/10.1016/j.cell.2012.01.035
1020 Coyte, K.Z., Rakoff-Nahoum, S., 2019. Understanding Competition and Cooperation within the
1021 Mammalian Gut Microbiome. Curr. Biol. 29, R538–R544.
1022 https://doi.org/10.1016/j.cub.2019.04.017
1023 Coyte, K.Z., Schluter, J., Foster, K.R., 2015. The ecology of the microbiome: Networks,
1024 competition, and stability. Science 350, 663–666.
1025 https://doi.org/10.1126/science.aad2602
1026 Danecek, P., Bonfield, J.K., Liddle, J., Marshall, J., Ohan, V., Pollard, M.O., Whitwham, A.,
1027 Keane, T., McCarthy, S.A., Davies, R.M., Li, H., 2021. Twelve years of SAMtools and
1028 BCFtools. GigaScience 10, giab008. https://doi.org/10.1093/gigascience/giab008
1029 Derrien, M., Vaughan, E.E., Plugge, C.M., Vos, W.M. de, 2004. Akkermansia muciniphila gen.
1030 nov., sp. nov., a human intestinal mucin-degrading bacterium. Int. J. Syst. Evol.
1031 Microbiol. 54, 1469–1476. https://doi.org/10.1099/ijs.0.02873-0
1032 Desai, M.S., Seekatz, A.M., Koropatkin, N.M., Kamada, N., Hickey, C.A., Wolter, M., Pudlo,
1033 N.A., Kitamoto, S., Terrapon, N., Muller, A., Young, V.B., Henrissat, B., Wilmes, P.,
1034 Stappenbeck, T.S., Núñez, G., Martens, E.C., 2016. A Dietary Fiber-Deprived Gut

1035 Microbiota Degrades the Colonic Mucus Barrier and Enhances Pathogen Susceptibility.
1036 Cell 167, 1339-1353.e21. https://doi.org/10.1016/j.cell.2016.10.043
1037 Earle, K.A., Billings, G., Sigal, M., Lichtman, J.S., Hansson, G.C., Elias, J.E., Amieva, M.R.,
1038 Huang, K.C., Sonnenburg, J.L., 2015. Quantitative Imaging of Gut Microbiota Spatial
1039 Organization. Cell Host Microbe 18, 478–488.
1040 https://doi.org/10.1016/j.chom.2015.09.002
1041 Escalante, N.K., Lemire, P., Tleugabulova, M.C., Prescott, D., Mortha, A., Streutker, C.J.,
1042 Girardin, S.E., Philpott, D.J., Mallevaey, T., 2016. The common mouse protozoa
1043 Tritrichomonas muris alters mucosal T cell homeostasis and colitis susceptibility. J. Exp.
1044 Med. 213, 2841–2850. https://doi.org/10.1084/jem.20161776
1045 Ferreyra, J.A., Wu, K.J., Hryckowian, A.J., Bouley, D.M., Weimer, B.C., Sonnenburg, J.L., 2014.
1046 Gut microbiota-produced succinate promotes C. Difficile infection after antibiotic
1047 treatment or motility disturbance. Cell Host Microbe 16, 770–777.
1048 https://doi.org/10.1016/j.chom.2014.11.003
1049 Fischbach, M.A., Sonnenburg, J.L., 2011. Eating for two: How metabolism establishes
1050 interspecies interactions in the gut. Cell Host Microbe 10, 336–347.
1051 https://doi.org/10.1016/j.chom.2011.10.002
1052 Hampl, V., Cepicka, I., Flegr, J., Tachezy, J., Kulda, J., 2007. Morphological and Molecular
1053 Diversity of the Monocercomonadid Genera Monocercomonas, Hexamastix, and
1054 Honigbergiella gen. nov. Protist 158, 365–383.
1055 https://doi.org/10.1016/j.protis.2007.02.003
1056 Holden, H.M., Rayment, I., Thoden, J.B., 2003. Structure and Function of Enzymes of the Leloir
1057 Pathway for Galactose Metabolism*. J. Biol. Chem. 278, 43885–43888.
1058 https://doi.org/10.1074/jbc.r300025200
1059 Hooper, L.V., Littman, D.R., Macpherson, A.J., 2012. Interactions between the microbiota and
1060 the immune system. Science 336, 1268–1273. https://doi.org/10.1126/science.1223490

1061 Howitt, M.R., Lavoie, S., Michaud, M., Blum, A.M., Tran, S.V., Weinstock, J.V., Gallini, C.A.,
1062 Redding, K., Margolskee, R.F., Osborne, L.C., Artis, D., Garrett, W.S., 2016. Tuft cells,
1063 taste-chemosensory cells, orchestrate parasite type 2 immunity in the gut. Science 351,
1064 1329–1333. https://doi.org/10.1126/science.aaf1648
1065 Iraporda, C., Errea, A., Romanin, D.E., Cayet, D., Pereyra, E., Pignataro, O., Sirard, J.C.,
1066 Garrote, G.L., Abraham, A.G., Rumbo, M., 2015. Lactate and short chain fatty acids
1067 produced by microbial fermentation downregulate proinflammatory responses in
1068 intestinal epithelial cells and myeloid cells. Immunobiology 220, 1161–1169.
1069 https://doi.org/10.1016/j.imbio.2015.06.004
1070 Ivanov, I.I., Atarashi, K., Manel, N., Brodie, E.L., Shima, T., Karaoz, U., Wei, D., Goldfarb, K.C.,
1071 Santee, C.A., Lynch, S.V., Tanoue, T., Imaoka, A., Itoh, K., Takeda, K., Umesaki, Y.,
1072 Honda, K., Littman, D.R., 2009. Induction of Intestinal Th17 Cells by Segmented
1073 Filamentous Bacteria. Cell 139, 485–498. https://doi.org/10.1016/j.cell.2009.09.033
1074 Kamada, N., Seo, S.U., Chen, G.Y., Núñez, G., 2013. Role of the gut microbiota in immunity
1075 and inflammatory disease. Nat. Rev. Immunol. 13, 321–335.
1076 https://doi.org/10.1038/nri3430
1077 Karin, E.L., Mirdita, M., Söding, J., 2020. MetaEuk—sensitive, high-throughput gene discovery,
1078 and annotation for large-scale eukaryotic metagenomics. Microbiome 8, 48.
1079 https://doi.org/10.1186/s40168-020-00808-x
1080 Kolmogorov, M., Yuan, J., Lin, Y., Pevzner, P.A., 2019. Assembly of long, error-prone reads
1081 using repeat graphs. Nat. Biotechnol. 37, 540–546. https://doi.org/10.1038/s41587-019-
1082 0072-8
1083 Langmead, B., Salzberg, S.L., 2012. Fast gapped-read alignment with Bowtie 2. Nat. Methods
1084 9, 357–359. https://doi.org/10.1038/nmeth.1923
1085 Lee, Y.-S., Kim, T.-Y., Kim, Y., Lee, S.-H., Kim, S., Kang, S.W., Yang, J.-Y., Baek, I.-J., Sung,
1086 Y.H., Park, Y.-Y., Hwang, S.W., O, E., Kim, K.S., Liu, S., Kamada, N., Gao, N., Kweon,

1087 M.-N., 2018. Microbiota-Derived Lactate Accelerates Intestinal Stem-Cell-Mediated
1088 Epithelial Development. Cell Host Microbe 24, 833-846.e6.
1089 https://doi.org/10.1016/j.chom.2018.11.002
1090 Lemoine, F., Correia, D., Lefort, V., Doppelt-Azeroual, O., Mareuil, F., Cohen-Boulakia, S.,
1091 Gascuel, O., 2019. NGPhylogeny.fr: new generation phylogenetic services for non-
1092 specialists. Nucleic Acids Res. 47, W260–W265. https://doi.org/10.1093/nar/gkz303
1093 Levy, M., Thaiss, C.A., Zeevi, D., Dohnalová, L., Zilberman-Schapira, G., Mahdi, J.A., David, E.,
1094 Savidor, A., Korem, T., Herzig, Y., Pevsner-Fischer, M., Shapiro, H., Christ, A.,
1095 Harmelin, A., Halpern, Z., Latz, E., Flavell, R.A., Amit, I., Segal, E., Elinav, E., 2015.
1096 Microbiota-Modulated Metabolites Shape the Intestinal Microenvironment by Regulating
1097 NLRP6 Inflammasome Signaling. Cell 163, 1428–1443.
1098 https://doi.org/10.1016/j.cell.2015.10.048
1099 Li, H., Durbin, R., 2009. Fast and accurate short read alignment with Burrows–Wheeler
1100 transform. Bioinformatics 25, 1754–1760. https://doi.org/10.1093/bioinformatics/btp324
1101 Liao, Y., Smyth, G.K., Shi, W., 2014. featureCounts: an efficient general purpose program for
1102 assigning sequence reads to genomic features. Bioinformatics 30, 923–930.
1103 https://doi.org/10.1093/bioinformatics/btt656
1104 Littman, D.R., Pamer, E.G., 2011. Role of the Commensal Microbiota in Normal and Pathogenic
1105 Host Immune Responses. Cell Host Microbe 10, 311–323.
1106 https://doi.org/10.1016/j.chom.2011.10.004
1107 Lombard, V., Ramulu, H.G., Drula, E., Coutinho, P.M., Henrissat, B., 2014. The carbohydrate-
1108 active enzymes database (CAZy) in 2013. Nucleic Acids Res. 42, D490–D495.
1109 https://doi.org/10.1093/nar/gkt1178
1110 Love, M.I., Huber, W., Anders, S., 2014. Moderated estimation of fold change and dispersion for
1111 RNA-seq data with DESeq2. Genome Biol. 15, 550. https://doi.org/10.1186/s13059-014-
1112 0550-8

1113 Lukeš, J., Stensvold, C.R., ková, K.J.-P. i, Parfrey, L.W., 2015. Are Human Intestinal
1114 Eukaryotes Beneficial or Commensals? 11, e1005039.
1115 https://doi.org/10.1371/journal.ppat.1005039
1116 Lynch, J.B., Sonnenburg, J.L., 2012. Prioritization of a plant polysaccharide over a mucus
1117 carbohydrate is enforced by a Bacteroides hybrid two-component system. Mol.
1118 Microbiol. 85, 478–491. https://doi.org/10.1111/j.1365-2958.2012.08123.x
1119 Malik, S.-B., Brochu, C.D., Bilic, I., Yuan, J., Hess, M., Logsdon, J.M., Carlton, J.M., 2011.
1120 Phylogeny of Parasitic Parabasalia and Free-Living Relatives Inferred from Conventional
1121 Markers vs. Rpb1, a Single-Copy Gene. PLoS ONE 6, e20774.
1122 https://doi.org/10.1371/journal.pone.0020774
1123 Manni, M., Berkeley, M.R., Seppey, M., Zdobnov, E.M., 2021. BUSCO: Assessing Genomic
1124 Data Quality and Beyond. Curr. Protoc. 1, e323. https://doi.org/10.1002/cpz1.323
1125 Martens, E.C., Chiang, H.C., Gordon, J.I., 2008. Mucosal glycan foraging enhances fitness and
1126 transmission of a saccharolytic human gut bacterial symbiont. Cell Host Microbe 4, 447–
1127 57. https://doi.org/10.1016/j.chom.2008.09.007
1128 Mazmanian, S.K., Round, J.L., Kasper, D.L., 2008. A microbial symbiosis factor prevents
1129 intestinal inflammatory disease. Nature 453, 620–625.
1130 https://doi.org/10.1038/nature07008
1131 Meshulam-Simon, G., Behrens, S., Choo, A.D., Spormann, A.M., 2007. Hydrogen Metabolism in
1132 *Shewanella oneidensis* MR-1. Appl. Environ. Microbiol. 73, 1153–1165.
1133 https://doi.org/10.1128/AEM.01588-06
1134 Morita, N., Umemoto, E., Fujita, S., Hayashi, A., Kikuta, J., Kimura, I., Haneda, T., Imai, T.,
1135 Inoue, A., Mimuro, H., Maeda, Y., Kayama, H., Okumura, R., Aoki, J., Okada, N., Kida,
1136 T., Ishii, M., Nabeshima, R., Takeda, K., 2019. GPR31-dependent dendrite protrusion of
1137 intestinal CX3CR1+ cells by bacterial metabolites. Nature 566, 110–114.
1138 https://doi.org/10.1038/s41586-019-0884-1

1139 Morris, C.F., McLean, D., Engleson, J.A., Fuerst, E.P., Burgos, F., Coburn, E., 2012. Some
1140 observations on the granivorous feeding behavior preferences of the house mouse (Mus
1141 musculus L.). mammalia 76, 209–218. https://doi.org/10.1515/mammalia-2011-0121
1142 Muller, M., Mentel, M., Hellemond, J.J. van, Henze, K., Woehle, C., Gould, S.B., Yu, R.Y.,
1143 Giezen, M. van der, Tielens, A.G.M., Martin, W.F., 2012. Biochemistry and Evolution of
1144 Anaerobic Energy Metabolism in Eukaryotes. Microbiol. Mol. Biol. Rev. 76, 444–495.
1145 https://doi.org/10.1128/mmbr.05024-11
1146 Nadjsombati, M.S., McGinty, J.W., Lyons-Cohen, M.R., Jaffe, J.B., DiPeso, L., Schneider, C.,
1147 Miller, C.N., Pollack, J.L., Gowda, G.A.N., Fontana, M.F., Erle, D.J., Anderson, M.S.,
1148 Locksley, R.M., Raftery, D., Moltke, J. von, 2018. Detection of Succinate by Intestinal
1149 Tuft Cells Triggers a Type 2 Innate Immune Circuit. Immunity 49, 33-41.e7.
1150 https://doi.org/10.1016/j.immuni.2018.06.016
1151 Nayfach, S., Shi, Z.J., Seshadri, R., Pollard, K.S., Kyrpides, N.C., 2019. New insights from
1152 uncultivated genomes of the global human gut microbiome. Nature 568, 505–510.
1153 https://doi.org/10.1038/s41586-019-1058-x
1154 Palmieri, N., Ramires, M. de J., Hess, M., Bilic, I., 2021. Complete genomes of the eukaryotic
1155 poultry parasite Histomonas meleagridis: linking sequence analysis with virulence /
1156 attenuation. BMC Genomics 22, 753. https://doi.org/10.1186/s12864-021-08059-2
1157 Parfrey, L.W., Walters, W.A., Knight, R., 2011. Microbial Eukaryotes in the Human Microbiome:
1158 Ecology, Evolution, and Future Directions. Front. Microbiol. 2, 153.
1159 https://doi.org/10.3389/fmicb.2011.00153
1160 Parfrey, L.W., Walters, W.A., Lauber, C.L., Clemente, J.C., Berg-Lyons, D., Teiling, C., Kodira,
1161 C., Mohiuddin, M., Brunelle, J., Driscoll, M., Fierer, N., Gilbert, J.A., Knight, R., 2014.
1162 Communities of microbial eukaryotes in the mammalian gut within the context of
1163 environmental eukaryotic diversity. Front. Microbiol. 5, 429.
1164 https://doi.org/10.3389/fmicb.2014.00298

1165 Park, S.-Y., Rao, C., Coyte, K.Z., Kuziel, G.A., Zhang, Y., Huang, W., Franzosa, E.A., Weng, J.-
1166 K., Huttenhower, C., Rakoff-Nahoum, S., 2022. Strain-level fitness in the gut microbiome
1167 is an emergent property of glycans and a single metabolite. Cell 185, 513-529.e21.
1168 https://doi.org/10.1016/j.cell.2022.01.002
1169 Patnode, M.L., Beller, Z.W., Han, N.D., Cheng, J., Peters, S.L., Terrapon, N., Henrissat, B.,
1170 Gall, S.L., Saulnier, L., Hayashi, D.K., Meynier, A., Vinoy, S., Giannone, R.J., Hettich,
1171 R.L., Gordon, J.I., 2019. Interspecies Competition Impacts Targeted Manipulation of
1172 Human Gut Bacteria by Fiber-Derived Glycans. Cell 179, 59-73.e13.
1173 https://doi.org/10.1016/j.cell.2019.08.011
1174 Petrin, D., Delgaty, K., Bhatt, R., Garber, G., 1998. Clinical and Microbiological Aspects
1175 ofTrichomonas vaginalis. Clin. Microbiol. Rev. 11, 300–317.
1176 https://doi.org/10.1128/cmr.11.2.300
1177 Porter, Nathan T, Martens, Eric C, 2017. The Critical Roles of Polysaccharides in Gut Microbial
1178 Ecology and Physiology.
1179 Rooks, M.G., Garrett, W.S., 2016. Gut microbiota, metabolites and host immunity. Nat. Publ.
1180 Group 16, 341–352. https://doi.org/10.1038/nri.2016.42
1181 Schneeberger, M., Everard, A., Gómez-Valadés, A.G., Matamoros, S., Ramírez, S., Delzenne,
1182 N.M., Gomis, R., Claret, M., Cani, P.D., 2015. Akkermansia muciniphila inversely
1183 correlates with the onset of inflammation, altered adipose tissue metabolism and
1184 metabolic disorders during obesity in mice. Sci. Rep. 5, 16643.
1185 https://doi.org/10.1038/srep16643
1186 Schneider, C., O'Leary, C.E., Moltke, J. von, Liang, H.E., Ang, Q.Y., Turnbaugh, P.J.,
1187 Radhakrishnan, S., Pellizzon, M., Ma, A., Locksley, R.M., 2018. A Metabolite-Triggered
1188 Tuft Cell-ILC2 Circuit Drives Small Intestinal Remodeling. Cell 174, 271-284.e14.
1189 https://doi.org/10.1016/j.cell.2018.05.014

1190 Segata, N., Izard, J., Waldron, L., Gevers, D., Miropolsky, L., Garrett, W.S., Huttenhower, C.,
1191 2011. Metagenomic biomarker discovery and explanation. Genome Biol. 12, R60.
1192 https://doi.org/10.1186/gb-2011-12-6-r60
1193 Smith, P.M., Howitt, M.R., Panikov, N., Michaud, M., Gallini, C.A., Bohlooly-Y, M., Glickman,
1194 J.N., Garrett, W.S., 2013. The Microbial Metabolites, Short-Chain Fatty Acids, Regulate
1195 Colonic Treg Cell Homeostasis. Science 341, 569–573.
1196 https://doi.org/10.1126/science.1241165
1197 Smits, S.A., Leach, J., Sonnenburg, E.D., Gonzalez, C.G., Lichtman, J.S., Reid, G., Knight, R.,
1198 Manjurano, A., Changalucha, J., Elias, J.E., Dominguez-Bello, M.G., Sonnenburg, J.L.,
1199 2017. Seasonal cycling in the gut microbiome of the Hadza hunter-gatherers of
1200 Tanzania. Science 357, 802–806. https://doi.org/10.1126/science.aan4834
1201 Sonnenburg, E.D., Smits, S.A., Tikhonov, M., Higginbottom, S.K., Sonnenburg, J.L., 2016. Diet-
1202 induced extinctions in the gut microbiota compound over generations. Nature 529, 212–
1203 215. https://doi.org/10.1038/nature16504
1204 Sonnenburg, E.D., Sonnenburg, J.L., 2014. Starving our Microbial Self: The Deleterious
1205 Consequences of a Diet Deficient in Microbiota-Accessible Carbohydrates. Cell Metab.
1206 20, 779–786. https://doi.org/10.1016/j.cmet.2014.07.003
1207 Sonnenburg, E.D., Zheng, H., Joglekar, P., Higginbottom, S.K., Firbank, S.J., Bolam, D.N.,
1208 Sonnenburg, J.L., 2010. Specificity of Polysaccharide Use in Intestinal Bacteroides
1209 Species Determines Diet-Induced Microbiota Alterations. Cell 141, 1241–1252.
1210 https://doi.org/10.1016/j.cell.2010.05.005
1211 Sonnenburg, J.L., 2005. Glycan foraging in vivo by an intestine-adapted bacterial symbiont.
1212 Science 307, 1952–1955. https://doi.org/10.1126/science.1108397
1213 Stark, D., Barratt, J., Chan, D., Ellis, J.T., 2016. Dientamoeba fragilis, the Neglected
1214 Trichomonad of the Human Bowel. Clin. Microbiol. Rev. 29, 553–580.
1215 https://doi.org/10.1128/cmr.00076-15

1216 Tailford, L.E., Crost, E.H., Kavanaugh, D., Juge, N., 2015. Mucin glycan foraging in the human
1217 gut microbiome. Front. Genet. 6, 81. https://doi.org/10.3389/fgene.2015.00081
1218 Tuncil, Y.E., Xiao, Y., Porter, N.T., Reuhs, B.L., Martens, E.C., Hamaker, B.R., 2017. Reciprocal
1219 Prioritization to Dietary Glycans by Gut Bacteria in a Competitive Environment Promotes
1220 Stable Coexistence. mBio 8, e01068-17. https://doi.org/10.1128/mbio.01068-17
1221 Walker, B.J., Abeel, T., Shea, T., Priest, M., Abouelliel, A., Sakthikumar, S., Cuomo, C.A., Zeng,
1222 Q., Wortman, J., Young, S.K., Earl, A.M., 2014. Pilon: An Integrated Tool for
1223 Comprehensive Microbial Variant Detection and Genome Assembly Improvement. PLoS
1224 ONE 9, e112963. https://doi.org/10.1371/journal.pone.0112963
1225 Wardman, J.F., Bains, R.K., Rahfeld, P., Withers, S.G., 2022. Carbohydrate-active enzymes
1226 (CAZymes) in the gut microbiome. Nat. Rev. Microbiol. 1–15.
1227 https://doi.org/10.1038/s41579-022-00712-1
1228 Westrop, G.D., Wang, L., Blackburn, G.J., Zhang, T., Zheng, L., Watson, D.G., Coombs, G.H.,
1229 2017. Metabolomic profiling and stable isotope labelling of Trichomonas vaginalis and
1230 Tritrichomonas foetus reveal major differences in amino acid metabolism including the
1231 production of 2-hydroxyisocaproic acid, cystathionine and S-methylcysteine. PLOS ONE
1232 12, e0189072. https://doi.org/10.1371/journal.pone.0189072
1233 Yang, Y.-W., Chen, M.-K., Yang, B.-Y., Huang, X.-J., Zhang, X.-R., He, L.-Q., Zhang, J., Hua,
1234 Z.-C., 2015. Use of 16S rRNA Gene-Targeted Group-Specific Primers for Real-Time
1235 PCR Analysis of Predominant Bacteria in Mouse Feces. Appl. Environ. Microbiol. 81,
1236 6749–6756. https://doi.org/10.1128/aem.01906-15
1237 Zhang, H., Yohe, T., Huang, L., Entwistle, S., Wu, P., Yang, Z., Busk, P.K., Xu, Y., Yin, Y.,
1238 2018. dbCAN2: a meta server for automated carbohydrate-active enzyme annotation.
1239 Nucleic Acids Res. 46, gky418. https://doi.org/10.1093/nar/gky418
1240 Zheng, Y., Paik, D., Yao, L., Kim, E., Trinath, J., Lu, J., Ha, S., Nelson, B.N., Kelly, S.P., Wu, L.,
1241 Zheng, Y., Longman, R.S., Rastinejad, F., Devlin, A.S., Krout, M.R., Fischbach, M.A.,

1242 Littman, D.R., Huh, J.R., 2019. Bile acid metabolites control TH17 and Treg cell
1243 differentiation. Nature 576, 143–148. https://doi.org/10.1038/s41586-019-1785-z
1244 Zinöcker, M.K., Lindseth, I.A., 2018. The Western Diet–Microbiome-Host Interaction and Its
1245 Role in Metabolic Disease. Nutrients 10, 365. https://doi.org/10.3390/nu10030365
1246
1247
1248
1249
1250
1251
1252
1253
1254
1255
1256
1257
1258
1259
1260
1261
1262
1263
1264
1265
1266
1267

1268 **Supplemental figure legends**

1269 **Figure S1. Discovery of *T. casperi*, a new species of murine commensal parabasalid,**
1270 **related to Figure 1**

1271 (A) Alignment of ITS sequences from *Tmu* and *Tc*. (B) Abundance of *Tmu* and *Tc* in the distal
1272 SI, cecum, and colon. Data is plotted as mean and each symbol represents an individual
1273 mouse. *p<0.05, ***p<0.001, NS, not significant by Mann-Whitney test.

1274

1275 **Figure S2. *Tmu* dominates tuft cell responses in the distal SI, and colonic responses are**
1276 **not adhesion-driven, related to Figure 2**

1277 (A) Tuft cell frequency in the epithelium of the distal SI of mice colonized by each protist
1278 individually, or colonized by both species. (B) Protist quantification in mice from (A). (C) Western
1279 Blot of *Tmu* and *Tc* lysates stained with the anti-*Tmu* polyclonal antibody. (D) Representative
1280 image of a *Tmu* trophozoite (left) and pseudocyst (right). Protists stained with anti-*Tmu* antibody
1281 (green), nuclei stained with DAPI (blue). Scale bars are 5μm. (E) Representative image of a
1282 *Tmu* cell adhered to the colonic epithelium. Scale bar is 10μm. (F) Representative image of a
1283 flushed colon from a *Tmu*-colonized mouse. *Tmu* stained with anti-*Tmu* antibody (green), mucus
1284 stained with UEA1 (red), nuclei stained with DAPI (blue), epithelium stained with E-Cadherin
1285 (white). Scale bar is 150μm. Data is plotted as mean and each symbol represents an individual
1286 mouse from three pooled experiments (A). **p<0.01, ***p<0.001, NS, not significant by Mann-
1287 Whitney test.

1288

1289 **Figure S3: Characterization of fermentative metabolic pathways in parabasalids, related**
1290 **to Figure 3**

1291 (A) Tuft cell frequency in the epithelium of the distal small intestine, in WT or *Gpr91*$^{-/-}$ mice
1292 colonized by each protist, or fed succinate in the drinking water. (B) Quantification of
1293 extracellular succinate in the cecal contents of mice colonized with each protist. (C) Genome

1294 assembly statistics for *Tmu* and *Tc* draft genomes. (D) Extracellular SCFA quantification in the
1295 cecal lumen of mice colonized by *Tc*. (E) Succinate (left) and lactate (right) quantification in
1296 culture supernatants of *P. hominis* (class *Trichomonadea*) and *M. colubrorum* (class
1297 *Tritrichomonadea*). Data is plotted as mean with SD in B, D, and E. The graph in A is plotted as
1298 the mean with each symbol representing an individual mouse pooled from two experiments.
1299 *p<0.05, **p<0.01, ***p<0.001, NS, not significant by Student's T test.
1300
1301 **Figure S4. *Tmu* and *Tc* occupy different nutritional niches within the microbiota, related**
1302 **to Figure 4**
1303 (A) Abundance of *Tmu* and (B) *Tc* in the cecal contents of mice fed diets with different fiber
1304 compositions for two weeks. Inulin and cellulose are the only fibers present in the defined chow.
1305 (C) 16S rRNA amplicon sequencing of the stool of mice with or without each protist. Each
1306 column represents the microbiome composition of a single mouse. (D) qPCR Quantification of
1307 total bacterial abundance in the stool of mice from (C). (E) Species richness in the stool of mice
1308 from (C). (F) Linear Discriminant Analysis scores showing microbiome changes associated with
1309 *Tmu* colonization. OTUs in green have higher abundance with *Tmu* colonization, OTUs in red
1310 have lower abundance with *Tmu* colonization. Data is plotted as mean in (A, B, and D), with
1311 each symbol representing an individual mouse pooled from two experiments. *p<0.05, **p<0.01,
1312 NS, not significant by Student's T test or Mann-Whitney test.
1313
1314 **Figure S5. Fiber deprivation causes *Tmu* to switch to a mucolytic metabolism, related to**
1315 **Figure 5**
1316 (A) Serial passaging of *Tmu* in PBF medium. Drops in culture density show when *Tmu* was
1317 subcultured into fresh media. (B) Survival of *Tc* in PBF medium after 24 hours, with maltose or
1318 mucus added as the carbon source. (C) Representative image of *Tmu* in the colon of a mouse
1319 fed cellulose chow and fed antibiotics in the drinking water. *Tmu* is stained with anti-*Tmu*

1320 antibody (green), mucus is stained with UEA1 (red), nuclei are stained with DAPI (blue). Scale
1321 bar is 100μm. (D) *Tmu* abundance in the stool of mice after two weeks of feeding on cellulose
1322 chow and different antibiotic treatments. (E) Quantification of total bacterial abundance in the
1323 stool of *Tmu*-colonized mice fed cellulose chow and given different antibiotic treatments in the
1324 drinking water (mice from Figure 5F). Graphs (A and B) depict mean and SD. Each symbol
1325 represents an individual mouse from three pooled experiments (D and E) *$p<0.05$, **$p<0.01$,
1326 NS, not significant by Mann-Whitney test.
1327
1328 **Figure S6. *Tmu* utilizes specific dietary fibers as a carbon source, Related to Figure 6**
1329 (A) *Tmu in vitro* growth curves with different dietary fibers in PBF medium. Dashed lines show
1330 maximum growth over 5 days in PBF medium without a supplemented carbon source. (B)
1331 Succinate quantification in the culture supernatants of *Tmu* cultured with maltose or mucus as a
1332 carbon source. Graphs show mean with SD. **$p<0.01$, NS, not significant by Student's T test or
1333 Mann-Whitney test.
1334
1335
1336
1337
1338
1339

Figure 1

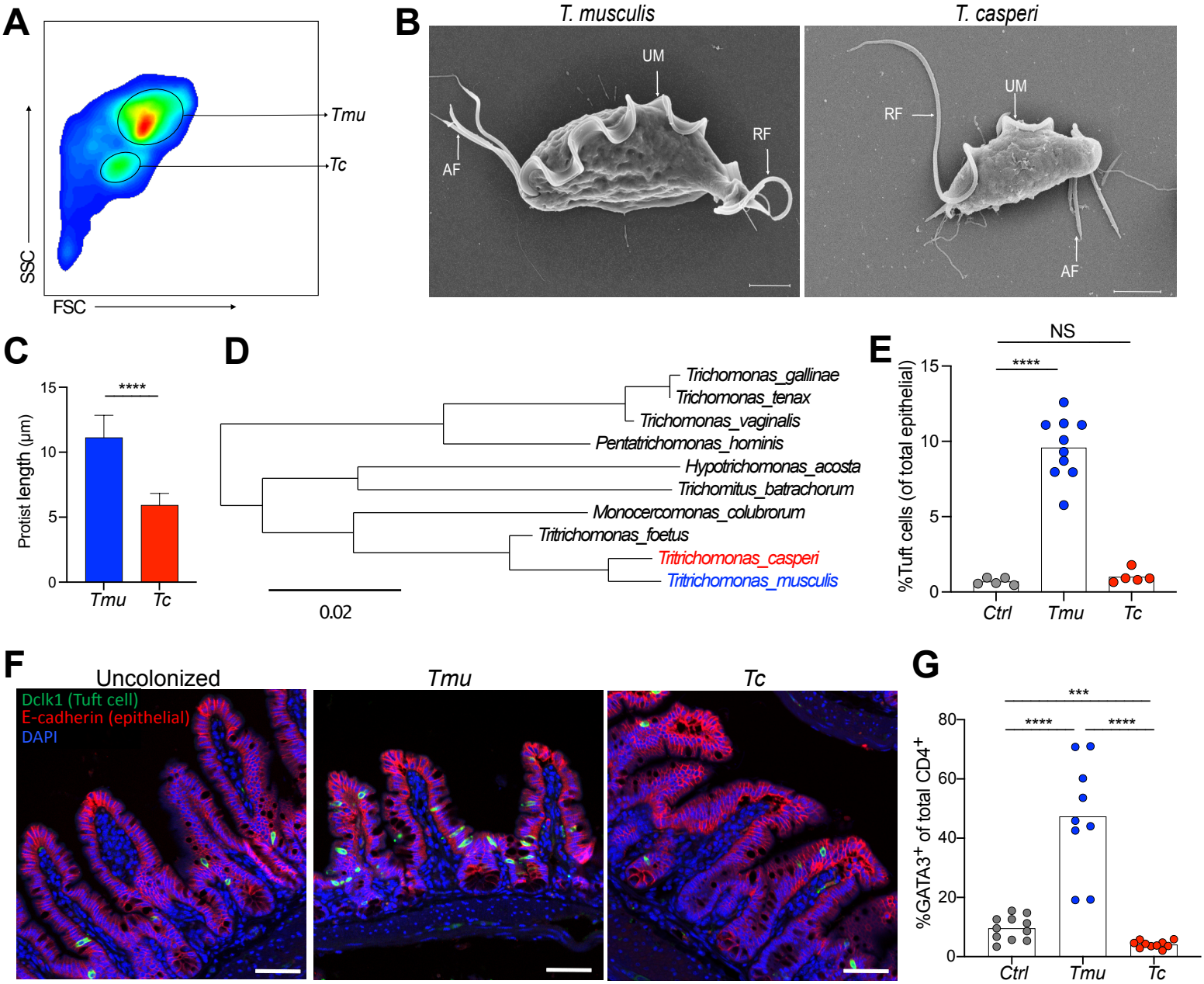
A
Tmu
Tc
SSC
FSC
B
T. musculis
T. casperi
UM
AF
RF
UM
RF
AF
C
****
Protist length (µm)
15
10
5
0
Tmu
Tc
D
Trichomonas_gallinae
Trichomonas_tenax
Trichomonas_vaginalis
Pentatrichomonas_hominis
Hypotrichomonas_acosta
Trichomitus_batrachorum
Monocercomonas_colubrorum
Tritrichomonas_foetus
Tritrichomonas_casperi
Tritrichomonas_musculis
0.02
E
NS
****
%Tuft cells (of total epithelial)
15
10
5
0
Ctrl
Tmu
Tc
F
Uncolonized
Tmu
Tc
Dclk1 (Tuft cell)
E-cadherin (epithelial)
DAPI
G
***
****
****
%GATA3+ of total CD4+
80
60
40
20
0
Ctrl
Tmu
Tc

Figure 2

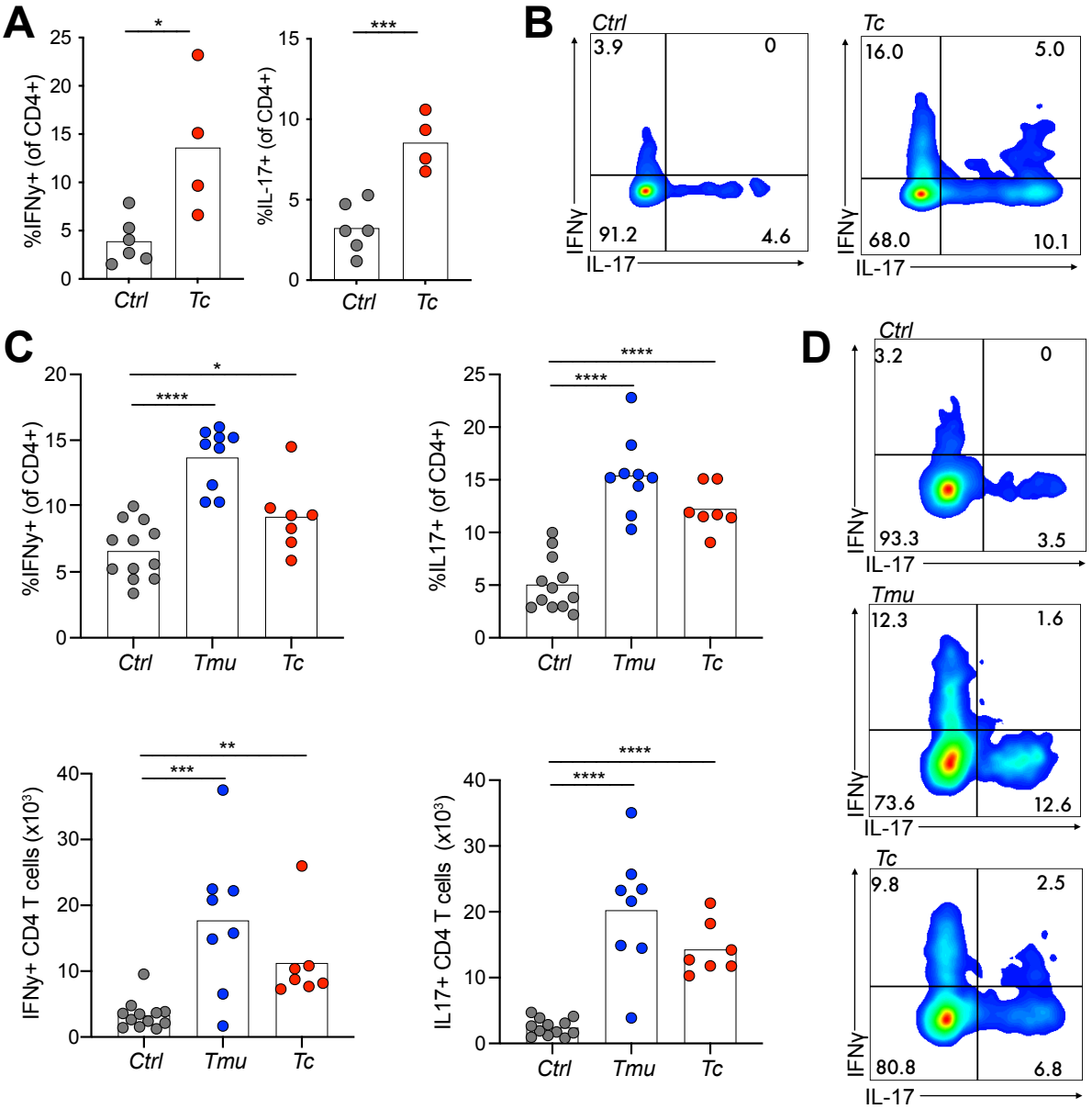
A
%IFNγ+ (of CD4+)
%IL-17+ (of CD4+)
Ctrl
Tc
B
Ctrl
3.9
0
91.2
4.6
Tc
16.0
5.0
68.0
10.1
IFNγ
IL-17
C
%IFNγ+ (of CD4+)
%IL17+ (of CD4+)
IFNγ+ CD4 T cells (x10³)
IL17+ CD4 T cells (x10³)
Ctrl
Tmu
Tc
D
Ctrl
3.2
0
93.3
3.5
Tmu
12.3
1.6
73.6
12.6
Tc
9.8
2.5
80.8
6.8
IFNγ
IL-17

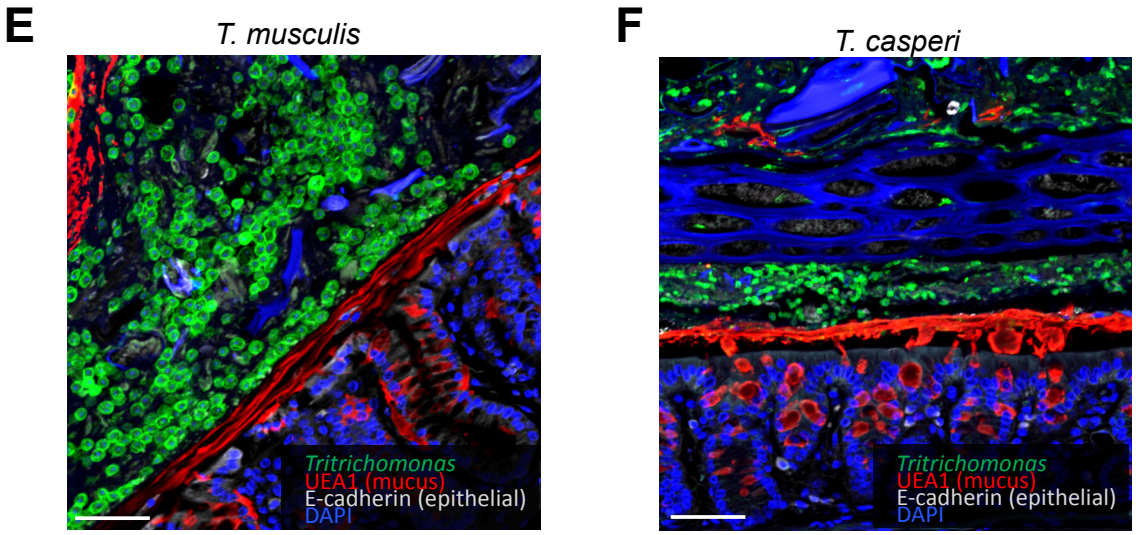
E
T. musculis
Tritrichomonas
UEA1 (mucus)
E-cadherin (epithelial)
DAPI
F
T. casperi
Tritrichomonas
UEA1 (mucus)
E-cadherin (epithelial)
DAPI

Figure 3

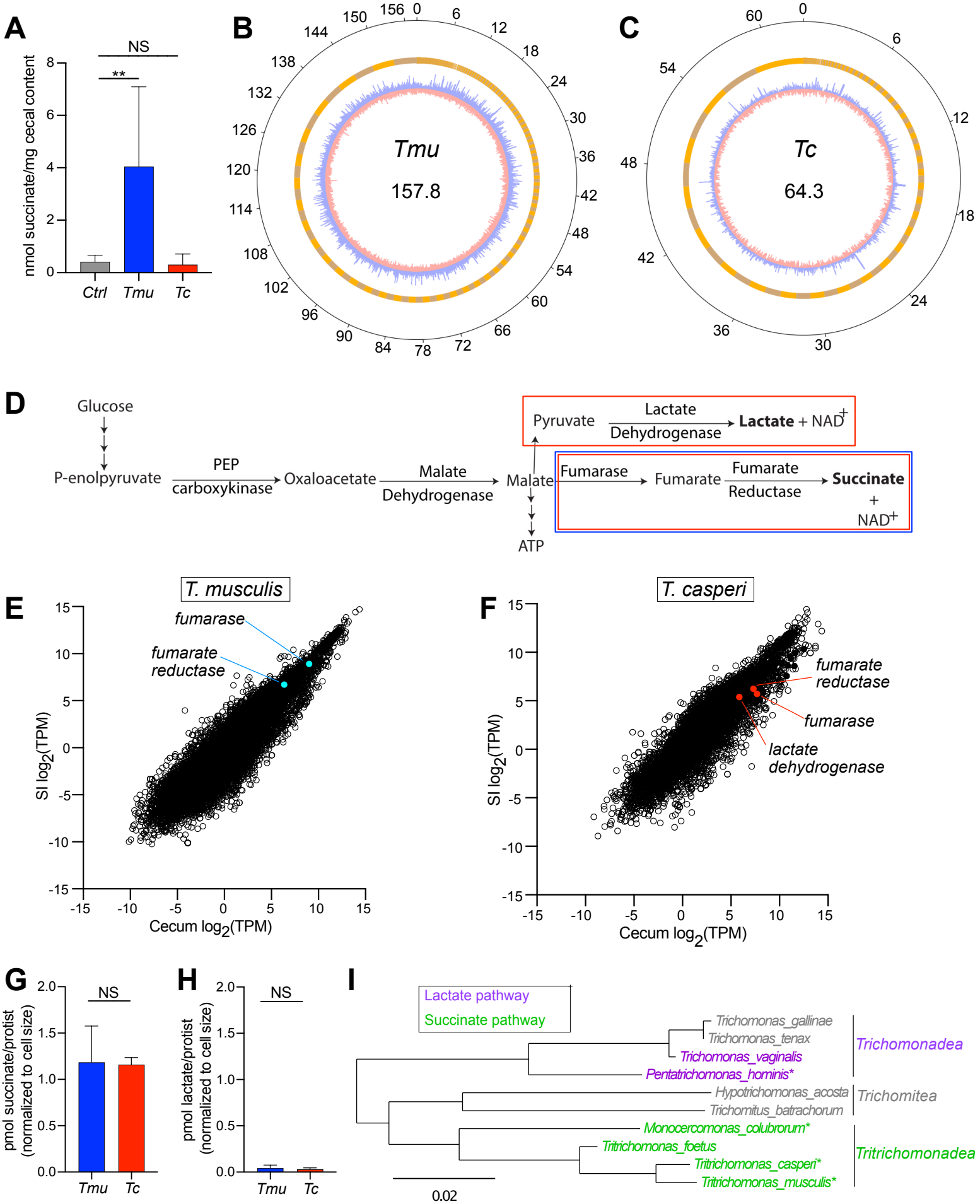
A
NS
**
nmol succinate/mg cecal content
Ctrl
Tmu
Tc
B
Tmu
157.8
C
Tc
64.3
D
Glucose
P-enolpyruvate
PEP carboxykinase
Oxaloacetate
Malate Dehydrogenase
Malate
ATP
Pyruvate
Lactate Dehydrogenase
Lactate + NAD+
Fumarase
Fumarate
Fumarate Reductase
Succinate + NAD+
E
T. musculis
fumarase
fumarate reductase
SI log2(TPM)
Cecum log2(TPM)
F
T. casperi
fumarate reductase
fumarase
lactate dehydrogenase
SI log2(TPM)
Cecum log2(TPM)
G
NS
pmol succinate/protist (normalized to cell size)
Tmu
Tc
H
NS
pmol lactate/protist (normalized to cell size)
Tmu
Tc
I
Lactate pathway
Succinate pathway
Trichomonas_gallinae
Trichomonas_tenax
Trichomonas_vaginalis
Pentatrichomonas_hominis*
Hypotrichomonas_acosta
Trichomitus_batrachorum
Monocercomonas_colubrorum*
Tritrichomonas_foetus
Tritrichomonas_casperi*
Tritrichomonas_musculis*
Trichomonadea
Trichomitea
Tritrichomonadea
0.02

Figure 4

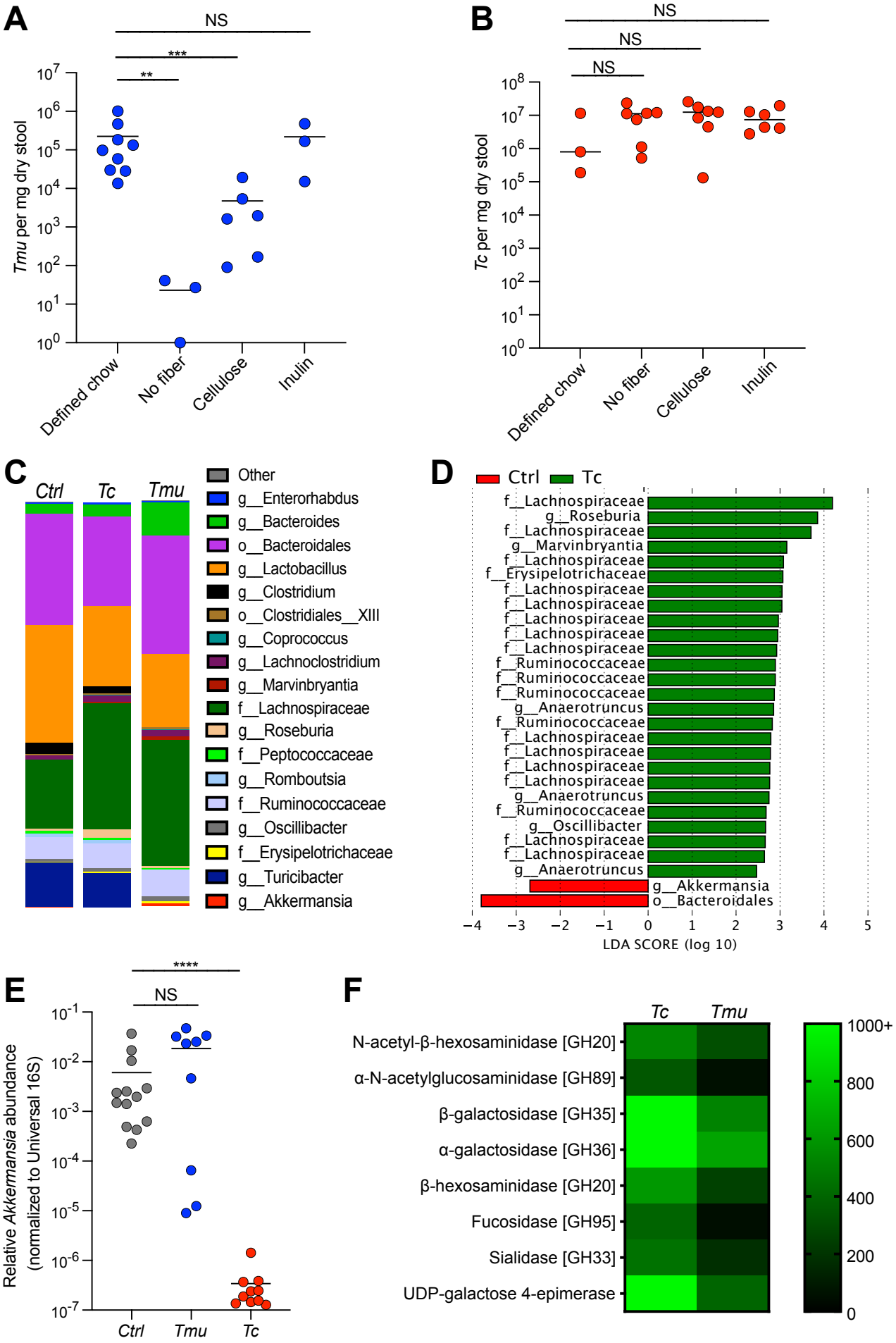
A
NS
***
**
Tmu per mg dry stool
Defined chow
No fiber
Cellulose
Inulin
B
NS
NS
NS
Tc per mg dry stool
Defined chow
No fiber
Cellulose
Inulin
C
Ctrl
Tc
Tmu
Other
g__Enterorhabdus
g__Bacteroides
o__Bacteroidales
g__Lactobacillus
g__Clostridium
o__Clostridiales__XIII
g__Coprococcus
g__Lachnoclostridium
g__Marvinbryantia
f__Lachnospiraceae
g__Roseburia
f__Peptococcaceae
g__Romboutsia
f__Ruminococcaceae
g__Oscillibacter
f__Erysipelotrichaceae
g__Turicibacter
g__Akkermansia
D
Ctrl
Tc
f__Lachnospiraceae
g__Roseburia
f__Lachnospiraceae
g__Marvinbryantia
f__Lachnospiraceae
f__Erysipelotrichaceae
f__Lachnospiraceae
f__Lachnospiraceae
f__Lachnospiraceae
f__Lachnospiraceae
f__Lachnospiraceae
f__Ruminococcaceae
f__Ruminococcaceae
f__Ruminococcaceae
g__Anaerotruncus
f__Ruminococcaceae
f__Lachnospiraceae
f__Lachnospiraceae
f__Lachnospiraceae
f__Lachnospiraceae
g__Anaerotruncus
f__Ruminococcaceae
g__Oscillibacter
f__Lachnospiraceae
f__Lachnospiraceae
g__Anaerotruncus
g__Akkermansia
o__Bacteroidales
LDA SCORE (log 10)
E
****
NS
Relative Akkermansia abundance
(normalized to Universal 16S)
Ctrl
Tmu
Tc
F
Tc
Tmu
N-acetyl-β-hexosaminidase [GH20]
α-N-acetylglucosaminidase [GH89]
β-galactosidase [GH35]
α-galactosidase [GH36]
β-hexosaminidase [GH20]
Fucosidase [GH95]
Sialidase [GH33]
UDP-galactose 4-epimerase
1000+
800
600
400
200
0

Figure 5

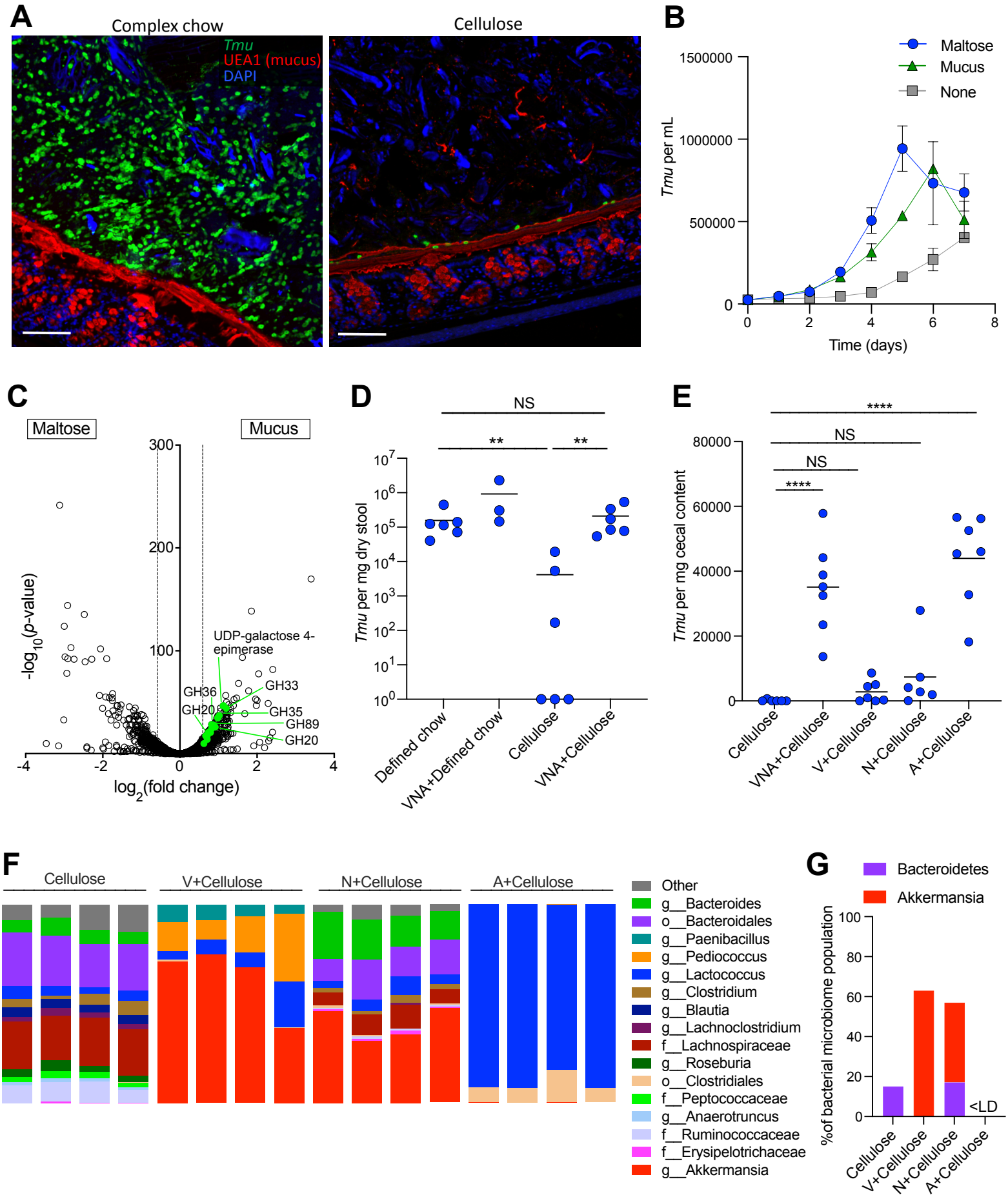
A
Complex chow
Cellulose
Tmu
UEA1 (mucus)
DAPI
B
Maltose
Mucus
None
Tmu per mL
1500000
1000000
500000
0
0
2
4
6
8
Time (days)
C
Maltose
Mucus
-log10(p-value)
300
200
100
UDP-galactose 4-epimerase
GH33
GH36
GH20
GH35
GH89
GH20
-4
-2
0
2
4
log2(fold change)
D
NS
**
**
Tmu per mg dry stool
Defined chow
VNA+Defined chow
Cellulose
VNA+Cellulose
E
****
NS
NS
****
Tmu per mg cecal content
80000
60000
40000
20000
0
Cellulose
VNA+Cellulose
V+Cellulose
N+Cellulose
A+Cellulose
F
Cellulose
V+Cellulose
N+Cellulose
A+Cellulose
Other
g__Bacteroides
o__Bacteroidales
g__Paenibacillus
g__Pediococcus
g__Lactococcus
g__Clostridium
g__Blautia
g__Lachnoclostridium
f__Lachnospiraceae
g__Roseburia
o__Clostridiales
f__Peptococcaceae
g__Anaerotruncus
f__Ruminococcaceae
f__Erysipelotrichaceae
g__Akkermansia
G
Bacteroidetes
Akkermansia
%of bacterial microbiome population
100
80
60
40
20
0
<LD
Cellulose
V+Cellulose
N+Cellulose
A+Cellulose

Figure 6

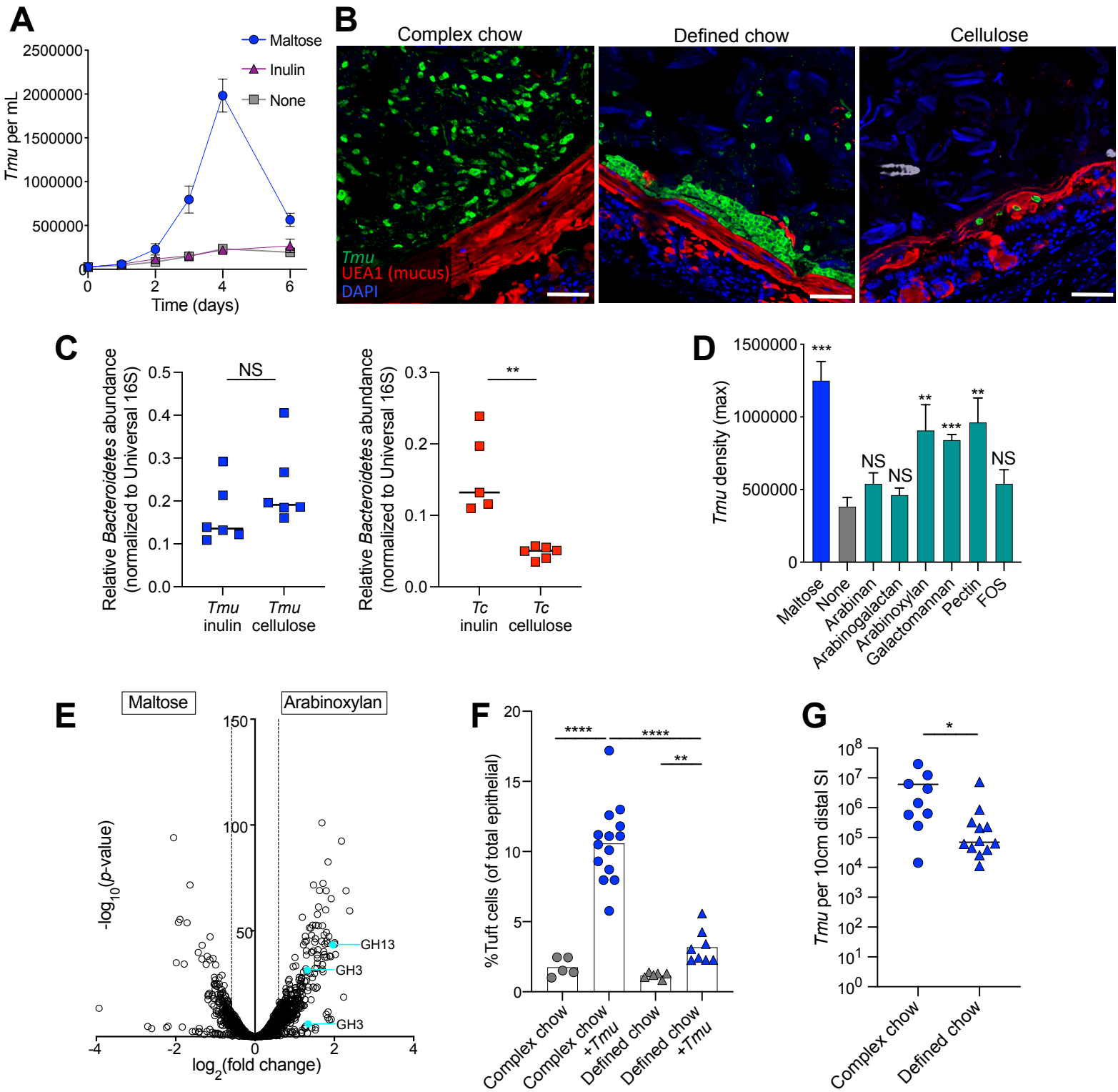
A
Maltose
Inulin
None
Tmu per mL
2500000
2000000
1500000
1000000
500000
0
0
2
4
6
Time (days)
B
Complex chow
Defined chow
Cellulose
Tmu
UEA1 (mucus)
DAPI
C
Relative Bacteroidetes abundance (normalized to Universal 16S)
NS
Tmu inulin
Tmu cellulose
**
Tc inulin
Tc cellulose
D
Tmu density (max)
1500000
1000000
500000
0
***
NS
NS
**
***
**
NS
Maltose
None
Arabinan
Arabinogalactan
Arabinoxylan
Galactomannan
Pectin
FOS
E
Maltose
Arabinoxylan
-log10(p-value)
log2(fold change)
GH13
GH3
GH3
F
%Tuft cells (of total epithelial)
****
****
**
Complex chow
Complex chow +Tmu
Defined chow
Defined chow +Tmu
G
Tmu per 10cm distal SI
*
Complex chow
Defined chow

Figure S1

A

```
MF375342/Tcasperi      TTCGTAAAAATTACTACAAACATATCTTTTTTTATAAGTAATAATAACATTTTCATACAA
Tmusculis              TTCGTAAATTTAATCACAAACATATTTTTT--------TAAAAAAAAAATTATCTAAAAT
                       ********  * *  ********** ****        *** ** ** *** **  * *

MF375342/Tcasperi      ACAAA-TAAATAACTAAATTAAAAAAATTAGACCTTAGGCAATGGATGTCTTGGCTTCTT
Tmusculis              ACAAATTAAATAATAAAAACAAAAAATTTAGACCTTAGGCAATGGATGTCTTGGCTTCTT
                       ***** *******  ***  ****** ********************************

MF375342/Tcasperi      ACACGAGGAAGAACGTTGCATAATGCGATAAGCGGCAGGAGTTGCTTTCATTGTGACATG
Tmusculis              ACACGAGGAAGAACGTTGCATAATGCGATAAGCGGCTGGAGTTGCTTACTTTGCGACAAG
                       ************************************ ********** * *** **** *

MF375342/Tcasperi      TTCGATCTTTGAATGCATATTGCGCGTAAGTTTGGGCTTTTGCTCAGACACGCATGTATG
Tmusculis              TTCGATCTTTGAATGCACATTGCGCGCCG--TCGAGCTTCGGCTTTGACACGCATATATG
                       ***************** ********     * * ****  ***  ********* ****

MF375342/Tcasperi      ATTCAGTAACCTATAATAATTTAAAGCAAATTCTCTTTTCTTGAAAAAGAGCGAAAAACT
Tmusculis              GTACAGTAACCCATAATAGTTTAAA--AAAATCTCTTTTTACGCAAAAGAGCGAAAAATT
                        * ******** ****** ******  *** ********   * ************** *

MF375342/Tcasperi      T---TATAAGCTTTTTAAGAA
Tmusculis              TATATGTAACCAACGTAA---
                       *   * *** *    ***
```

B

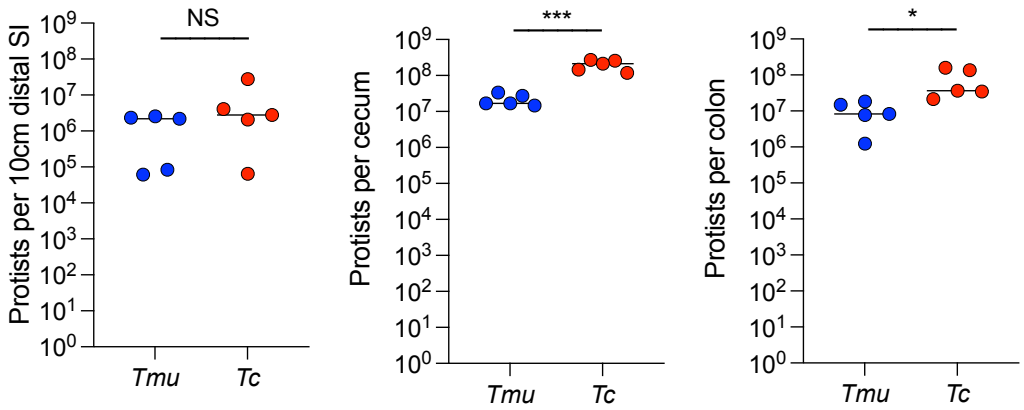

Figure S2

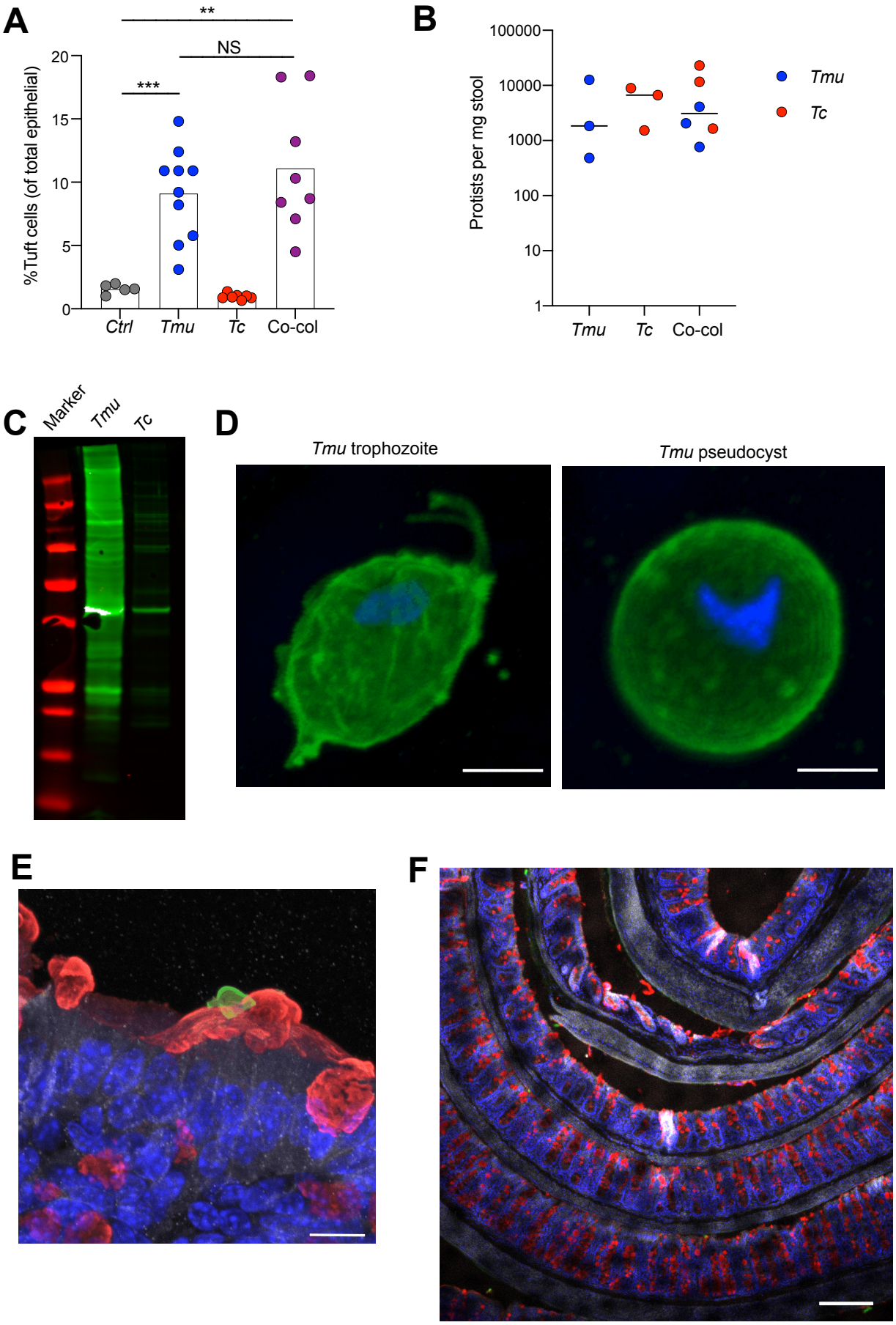
A
**
NS
***
%Tuft cells (of total epithelial)
20
15
10
5
0
Ctrl
Tmu
Tc
Co-col
B
100000
10000
1000
100
10
1
Protists per mg stool
Tmu
Tc
Co-col
Tmu
Tc
C
Marker
Tmu
Tc
D
Tmu trophozoite
Tmu pseudocyst
E
F

Figure S3

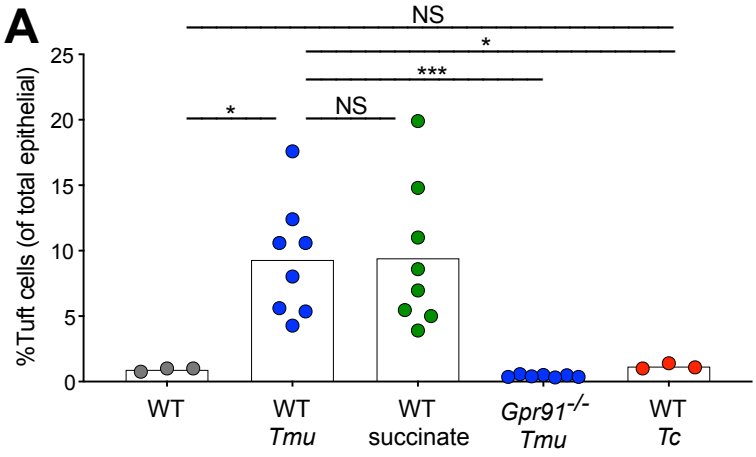

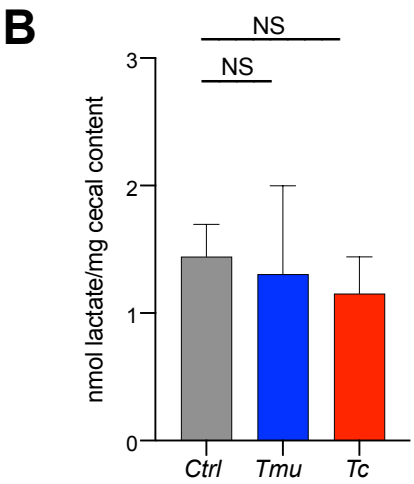

C

	T. musculis	*T. casperi*
Genome length (Mbp)	157.8	64.3
Gene count	45,134	22,632
N_{50} (Mbp)	1.477	1.213
Coverage	56.5	66.5

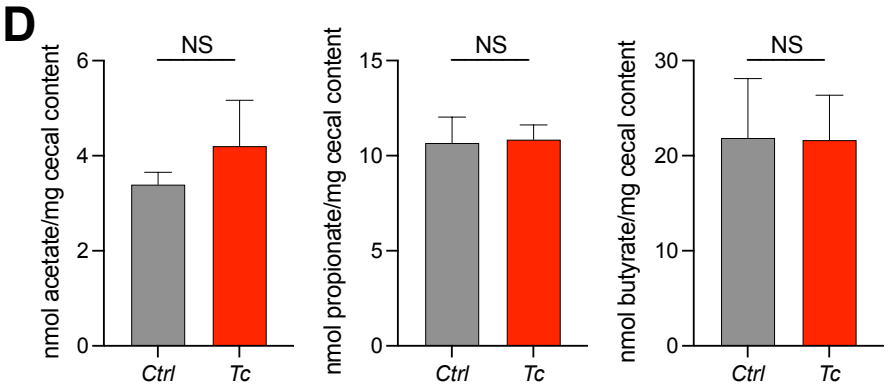

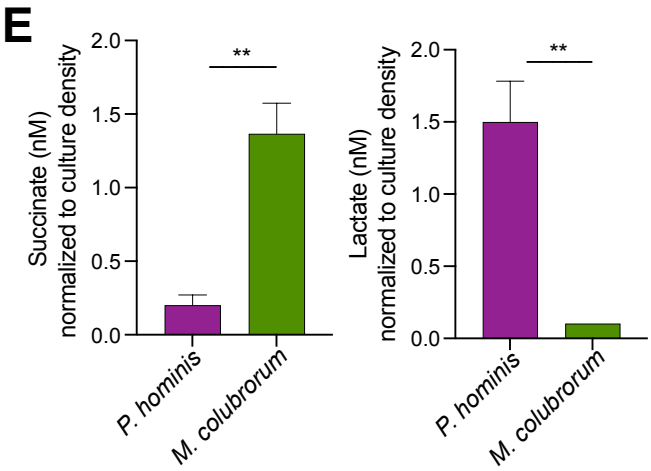

Figure S4

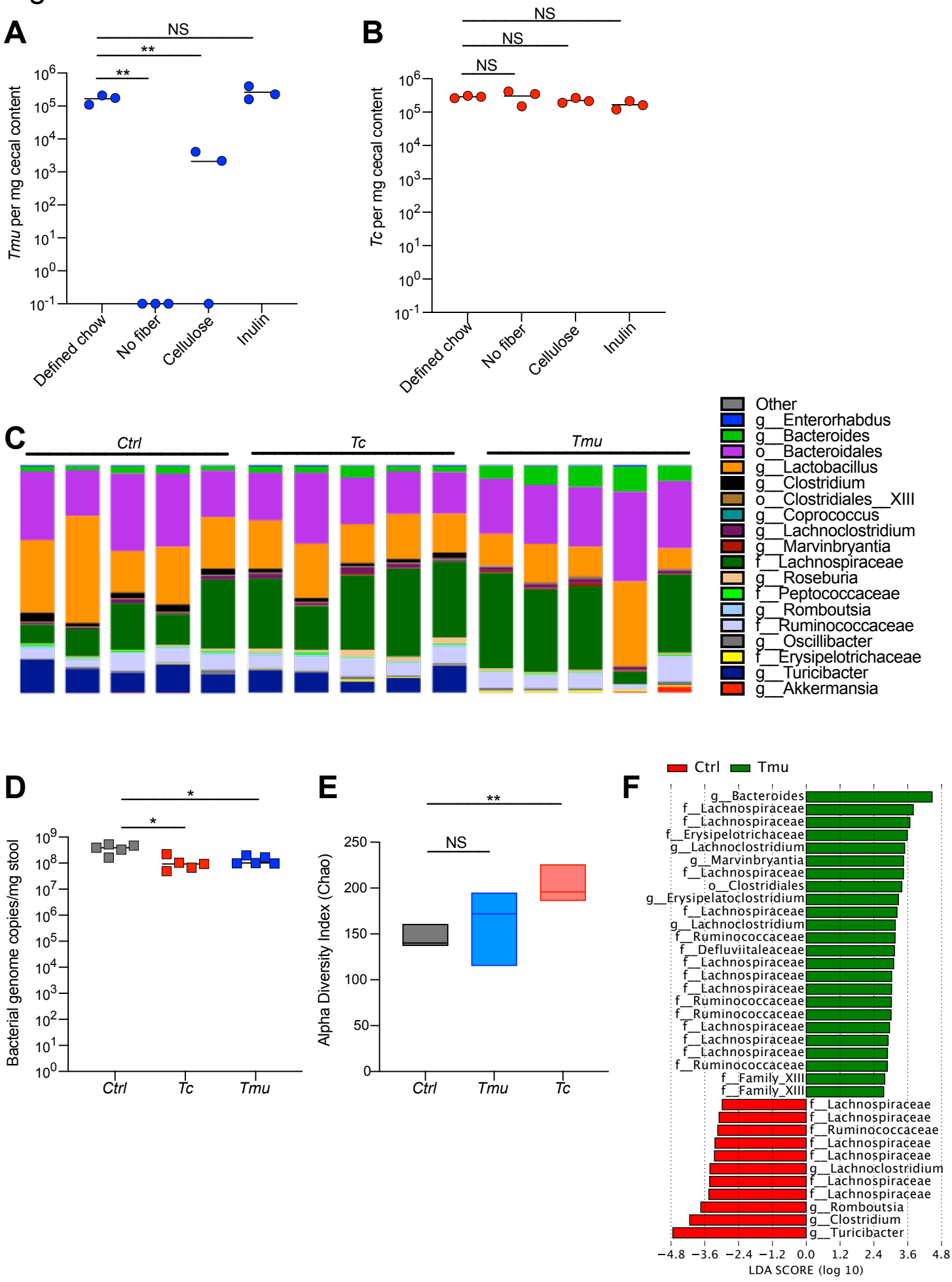
A
NS
**
**
Tmu per mg cecal content
Defined chow
No fiber
Cellulose
Inulin
B
NS
NS
NS
Tc per mg cecal content
Defined chow
No fiber
Cellulose
Inulin
C
Ctrl
Tc
Tmu
Other
g__Enterorhabdus
g__Bacteroides
o__Bacteroidales
g__Lactobacillus
g__Clostridium
o__Clostridiales__XIII
g__Coprococcus
g__Lachnoclostridium
g__Marvinbryantia
f__Lachnospiraceae
g__Roseburia
f__Peptococcaceae
g__Romboutsia
f__Ruminococcaceae
g__Oscillibacter
f__Erysipelotrichaceae
g__Turicibacter
g__Akkermansia
D
*
*
Bacterial genome copies/mg stool
Ctrl
Tc
Tmu
E
**
NS
Alpha Diversity Index (Chao)
Ctrl
Tmu
Tc
F
Ctrl
Tmu
g__Bacteroides
f__Lachnospiraceae
f__Lachnospiraceae
f__Erysipelotrichaceae
g__Lachnoclostridium
g__Marvinbryantia
f__Lachnospiraceae
o__Clostridiales
g__Erysipelatoclostridium
f__Lachnospiraceae
g__Lachnoclostridium
f__Ruminococcaceae
f__Defluviitaleaceae
f__Lachnospiraceae
f__Lachnospiraceae
f__Lachnospiraceae
f__Ruminococcaceae
f__Ruminococcaceae
f__Lachnospiraceae
f__Lachnospiraceae
f__Lachnospiraceae
f__Ruminococcaceae
f__Family_XIII
f__Family_XIII
f__Lachnospiraceae
f__Lachnospiraceae
f__Ruminococcaceae
f__Lachnospiraceae
f__Lachnospiraceae
g__Lachnoclostridium
f__Lachnospiraceae
f__Lachnospiraceae
g__Romboutsia
g__Clostridium
g__Turicibacter
LDA SCORE (log 10)

Figure S5

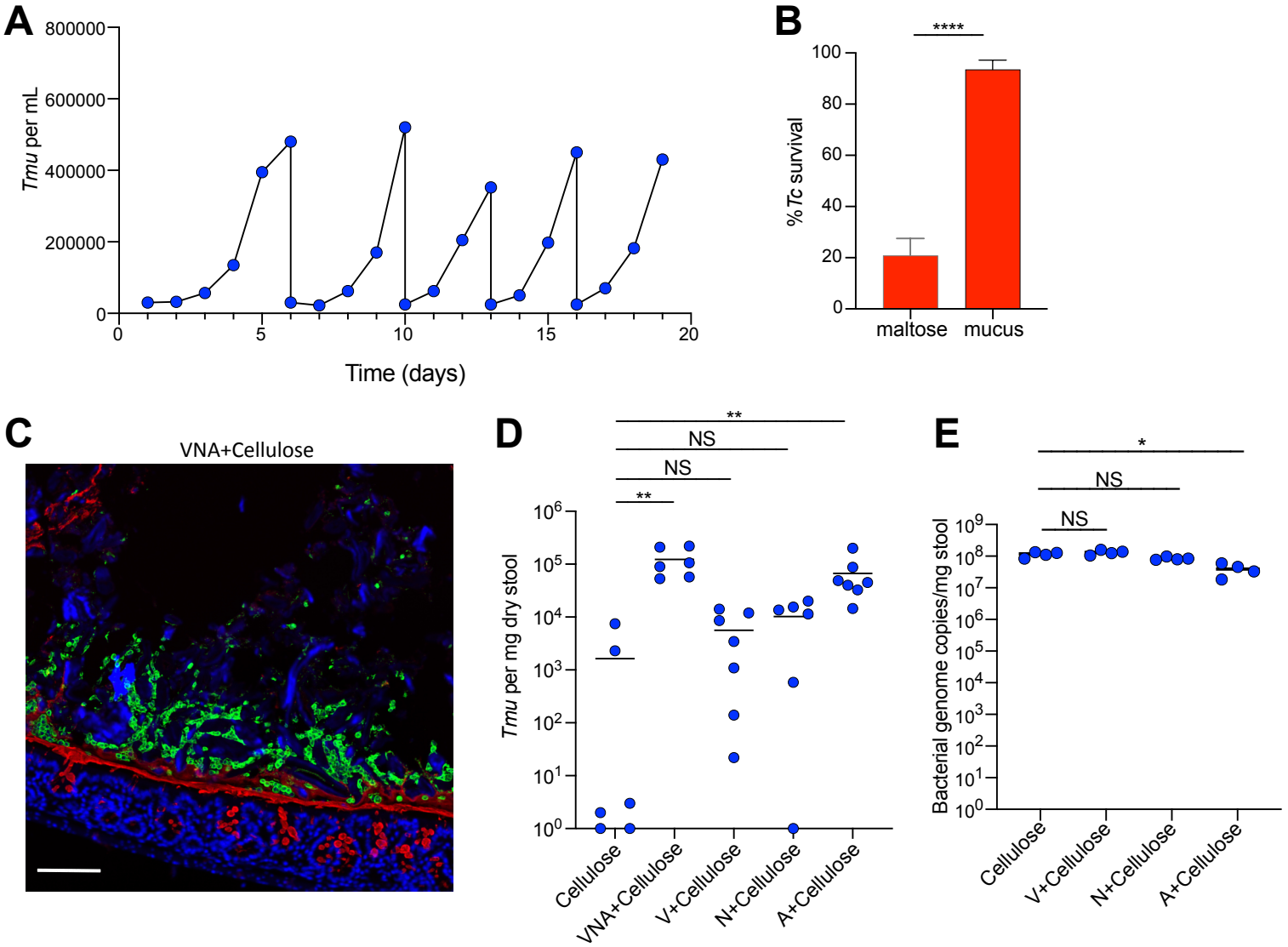
A
800000
600000
400000
200000
0
Tmu per mL
0
5
10
15
20
Time (days)
B
****
100
80
60
40
20
0
% Tc survival
maltose
mucus
C
VNA+Cellulose
D
**
NS
NS
**
10^6
10^5
10^4
10^3
10^2
10^1
10^0
Tmu per mg dry stool
Cellulose
VNA+Cellulose
V+Cellulose
N+Cellulose
A+Cellulose
E
*
NS
NS
10^9
10^8
10^7
10^6
10^5
10^4
10^3
10^2
10^1
10^0
Bacterial genome copies/mg stool
Cellulose
V+Cellulose
N+Cellulose
A+Cellulose

Figure S6

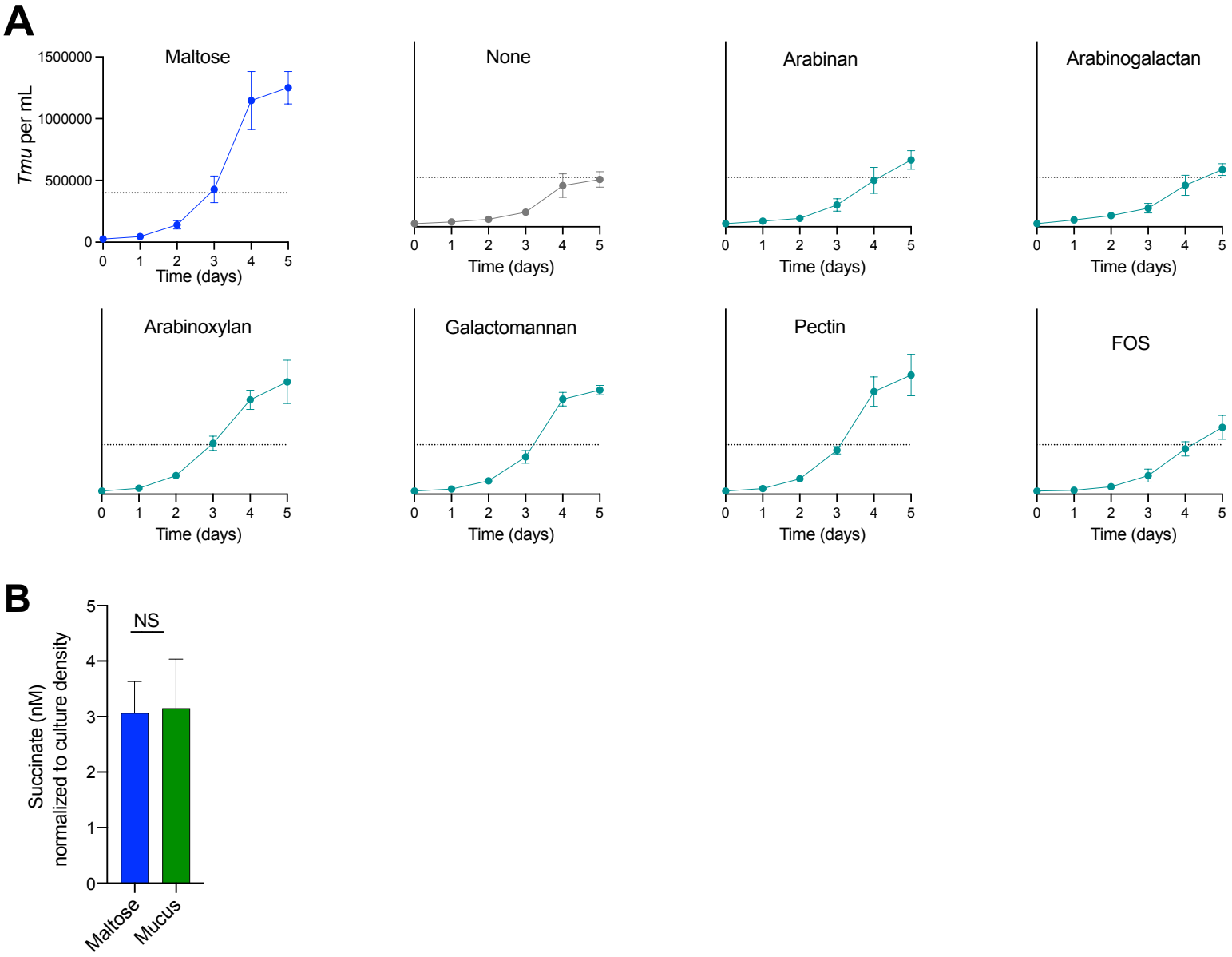
A
Maltose
None
Arabinan
Arabinogalactan
Arabinoxylan
Galactomannan
Pectin
FOS
Tmu per mL
1500000
1000000
500000
0
0 1 2 3 4 5
Time (days)
B
NS
Succinate (nM)
normalized to culture density
5
4
3
2
1
0
Maltose
Mucus